Journal of Biomedical Optics

BiomedicalOptics.SPIEDigitalLibrary.org

Raman spectroscopy of human skin: looking for a quantitative algorithm to reliably estimate human age

Giuseppe Pezzotti
Marco Boffelli
Daisuke Miyamori
Takeshi Uemura
Yoshinori Marunaka
Wenliang Zhu
Hiroshi Ikegaya

SPIE.

Raman spectroscopy of human skin: looking for a quantitative algorithm to reliably estimate human age

Giuseppe Pezzotti,[a,b,c,d,*] Marco Boffelli,[a] Daisuke Miyamori,[e] Takeshi Uemura,[e] Yoshinori Marunaka,[d] Wenliang Zhu,[f] and Hiroshi Ikegaya[e,*]
[a]Kyoto Institute of Technology, Ceramic Physics Laboratory, Sakyo-ku, Matsugasaki, Kyoto 606-8126, Japan
[b]Loma Linda University, Department of Orthopedic Research, Department of Orthopaedics, 11406 Loma Linda Drive, Suite 606 Loma Linda, California 92354, United States
[c]Osaka University, Center for Advanced Medical Engineering and Informatics, Yamadaoka, Suita, Osaka 565-0871, Japan
[d]Kyoto Prefectural University of Medicine, Department of Molecular Cell Physiology, Graduate School of Medical Science, Kamigyo-ku, 465 Kajii-cho, Kawaramachi dori, Kyoto 602-0841, Japan
[e]Kyoto Prefectural University of Medicine, Department of Forensic Medicine, Kamigyo-ku, 465 Kajii-cho, Kawaramachi dori, Kyoto 602-0841, Japan
[f]Osaka University, Department of Medical Engineering for Treatment of Bone and Joint Disorders, 2-2 Yamadaoka, Suita, Osaka 565-0854, Japan

Abstract. The possibility of examining soft tissues by Raman spectroscopy is challenged in an attempt to probe human age for the changes in biochemical composition of skin that accompany aging. We present a proof-of-concept report for explicating the biophysical links between vibrational characteristics and the specific compositional and chemical changes associated with aging. The actual existence of such links is then phenomenologically proved. In an attempt to foster the basics for a quantitative use of Raman spectroscopy in assessing aging from human skin samples, a precise spectral deconvolution is performed as a function of donors' ages on five cadaveric samples, which emphasizes the physical significance and the morphological modifications of the Raman bands. The outputs suggest the presence of spectral markers for age identification from skin samples. Some of them appeared as authentic "biological clocks" for the apparent exactness with which they are related to age. Our spectroscopic approach yields clear compositional information of protein folding and crystallization of lipid structures, which can lead to a precise identification of age from infants to adults. Once statistically validated, these parameters might be used to link vibrational aspects at the molecular scale for practical forensic purposes. [DOI: 10.1117/1.JBO.20.6.065008]

Keywords: Raman spectroscopy; human skin; human age estimate; protein folding; lipid crystallization.

Paper 150140R received Mar. 9, 2015; accepted for publication May 18, 2015; published online Jun. 25, 2015.

1 Introduction

In the vibrational spectra of biological molecules, indelible "fingerprints" can be found for the occurrence (and frequency) of a number of otherwise hidden natural phenomena. The discovery and rationalization of such spectral "fingerprints" represents a socially useful and fascinating practice, but also pose formidable challenges to spectroscopists. Unlike simpler inorganic structures, an explicit description of the irreducible phonon representation for complicated organic molecules is a task of enormous cumbersomeness, which can by no means be accomplished without the help of computational programs. Even an "elementary" protein structure possesses a number of distinct vibrational modes (i.e., in the order of 10^4),[1] which makes the task of unfolding such a structural complexity one of the hardest challenges in modern science. On the positive side, however, there is the high sensitivity of vibrational spectroscopy to structural features. This method can be exceptionally sensitive to even quite small variations of bond strength, i.e., in the order of 0.02%.[2] Such variations can promptly be resolved by probing with a spectral resolution better than 5 cm^{-1}, and modern spectroscopes usually possess spectral resolutions at least 1 order of magnitude better than the above threshold. In other words, Raman spectroscopy provides us with a suitably high sensitivity for monitoring subtle bond modifications and molecular distortions with high accuracy.

From an analytical point of view, the main consequence of the complexity of biomolecules has been that Raman spectra have often been treated as a mere matricial sequence of mathematical data, with little emphasis being placed on the interpretation of the physical origin of individual bands in the recorded spectra. Such a statistically driven approach could be quite useful in locating spectral differences. However, despite the huge piece of information potentially contained in the Raman spectra, such spectroscopic "cryptograms" have, most of the time, remained unfolded with only a small (qualitative) part of their contents being physically interpreted. On the other hand, several research groups have continued to intensely work on basic interpretations of the Raman spectra emitted from biological samples.[3–9] Such basic approaches have enabled

*Address all correspondence to: Giuseppe Pezzotti, E-Mail: pezzotti@kit.ac.jp; Hiroshi Ikegaya, E-mail: ikegaya@koto.kpu-m.ac.jp

1083-3668/2015/$25.00 © 2015 SPIE

clarifying a number of structural features in organic molecules, including the interpretation of Raman bands and their spectral positions from saccharides,[5] lipids[3,4,10] and carotenoids.[9] The presence of mono-unsaturated acyl groups has also been related to the first derivative value of scattering intensities measured at 1656 cm^{-1}, which relate to the vibrational stretching of *cis* and *trans* C=C bonds in lipids.[10] Moreover, classification overviews of Raman spectra for biomolecules have recently become available.[11] Specifically regarding model protein structures, Raman bands represent vibrational modes of both the peptide backbone and its side chains. Spectral positions, intensities and polarizations of the Raman bands result in being quite sensitive to protein secondary, tertiary and quaternary structures, in addition to side-chain orientations and local environments. In a number of favorable cases, the Raman spectrum has provided a straightforward signature of the protein three-dimensional (3-D) structure, intramolecular dynamics and intermolecular interactions.[12] Specifically related to skin, its constituent organic molecules generally display in the Raman spectrum according to the corresponding model structures, but significant compositional and structural variations can be expected with progressing age. Collagen fibers are composed of collagen types I and III in a ratio that depends on their location being either in the papillary or in the reticular dermis. In young people, collagen fibers in the region of papillary dermis take the form of densely packed and irregularly arranged networks, whereas in the reticular dermis, their morphology appears coarser and with loosely arranged and intertwined bundles. Upon aging, the amount of collagen fibers increases, packing becomes denser, and the stereological arrangement is less twisted.[13,14] Moreover, elastic fibers consist of an amorphous fraction (~90% of the mature fiber), which is exclusively composed of elastin and a microfibrillar component consisting of nanostructured fibrils.[15] Superficial microfibril bundles gradually thicken and merge with increasingly large amounts of amorphous elastin as the papillary dermis changes into reticular dermis. However, with increasing age, the concentration of elastin fibers in the papillary dermis decreases. Accordingly, fibers from the skin of older individuals lose some of their elasticity, thicken (fold) into agglutinated masses and unravel.[14] While the anatomical details of structural skin modifications with aging are well studied and documented, methods for finding such features in the recorded Raman spectra are yet at their early development. Consequences of aging processes are obviously the changes in the biochemical structure of tissue, which should also be seen in its Raman spectrum. The challenge, therefore, shifts now to how to translate such qualitative notions into a quantitative spectroscopic algorithm capable of assessing human age to a degree of precision.

Building upon previous outputs of different approaches to Raman evaluations of biological samples, we challenged, in this paper, the establishment of parameters for the quantitative assessment of human age from skin samples belonging to cadaveric donors. This study was mainly motivated by the need in the field of forensic pathology to determine within an improved degree of accuracy the age of human subjects lacking specific identity information. Spectroscopic outputs were rationalized and discussed in terms of selected parameters, including the degree of protein folding and the degree of lipid crystallization. Some other parameters—such as the fractional ratio between α-helix and β-sheet, the presence of sphingomyelin in the ceramide structure, and the content of collagen versus lipids—were also noticed. It should be stated at the outset of our awareness that this study lacks statistical relevance, which has been a direct consequence of the cadaveric origin of the studied samples and the need to examine the skin sample within a narrow interval of time (i.e., <1 week) since the date of decease and the necessity of preliminary clearing up ethical issues with respect to donors. Nevertheless, specific care was taken in obtaining "standard" spectra for each donor with averaging on a large number of acquisitions on each sample. In other words, the validity of the shown concepts relies on the basic assumption that if an age representing parameter (i.e., a "natural clock") actually exists in the vibrational behavior of skin tissue, this should be independent of individual classes. The practical possibility of retrieving age information from skin samples is a confirmation that sensitive and selective "fingerprints" of natural aging exist in the intermolecular interactions and dynamics of the constituent phases of human skin. Further studies are presently ongoing for obtaining a statistical validation of the proposed parameters and procedures.

2 Experimental Procedures

A series of cadaveric skin samples was obtained from donors (human patients deceased at different ages spanning from a few months to 62 years old) upon preliminary clearance of ethical procedures at the Department of Forensic Medicine of the Graduate School of Medical Science of Kyoto Prefectural University of Medicine. Details of the cadaver samples available for this study are provided in Table 1. The samples were taken from abdominal locations in the body unexposed to solar irradiation. Skin samples were typically 10×10 mm^2 wide (cut by hand) and encompassed the full thickness of the skin structure, from the stratum corneum to the hypodermis. All the skin samples investigated in this study belonged to the same race, showing similar color (pale white skin, with some yellow tones) on the skin surface. No special medical treatments were performed on the skin samples before and after they were extracted from the human bodies. More importantly, all the donors examined in this study died in a healthy situation and their pathological records did not show specific items either related to liver or other diseases specifically impacting on protein and lipid structures. Neither the infant nor other donors received medical therapy that might have induced changes in the molecular structure of their skin. Raman experiments were conducted on the skin samples within less than 1 week after the date of the patient's decease. The skin samples were preserved at −70°C in a freezer before Raman analysis. Immediately before the Raman experiments, skin samples were thawed and kept on ice. Prior to Raman spectroscopic characterizations, each

Table 1 Information on the human cadaver samples investigated in this study.

Sample	Age	Sex	Cause of death
1	3 months	Female	Aspiration asphyxia
2	15 years	Male	Hemorrhagic shock
3	17 years	Male	Drowning
4	35 years	Male	Drowning
5	61 years	Male	Cardiac rupture

sample was divided into smaller specimens and hematoxylin and eosin (H&E) stain histology and optical microscopy were applied on the cross sections of one specimen for each sample in order to preliminarily assess the location of different zones of epidermis and dermis from morphological features. As a spectroscopic reference, a sample of skin type I collagen was also investigated, which was purchased from Sigma-Aldrich, Co.[16]

All the Raman spectroscopic experiments described in this paper were carried out in backscattering optical probe configuration with using a triple monochromator (T-64000, Horiba/Jobin-Yvon, Kyoto, Japan) equipped with a liquid nitrogen-cooled charge coupled device. The excitation source in the present experiments used a 532-nm $Nd:YVO_4$ diode-pumped solid-state laser (SOC JUNO, Showa Optronics Co. Ltd., Tokyo, Japan) operating with a power of 200 mW. An objective lens with a numerical aperture of 0.5 was used both to focus the laser beam on the sample surface and to collect the scattered Raman light. All the experiments described in this paper were conducted with a pinhole aperture of 100 μm and by employing an objective lens with a magnification of 100×. All the experiments were conducted at room temperature with a relative humidity of 68%. Each spectrum at a measurement location was collected for five scans with the accumulation time of each scan being 1 min. For each studied sample, several tens of spectra were collected on the top skin surface and an average spectrum could be obtained with a statistical validity using commercial software (LabSpec Ver. 4.02, Jobin-Ivon/Horiba, Tokyo, Japan). On the cross section of each skin sample, spectral line scans were also performed, starting from the stratum corneum to 800 μm deep in the depth direction. Spectral Raman lines were analyzed using a commercially available software package (Origin 9.1, OriginLab Co., Northampton, Massachusetts, United States). Fitting was performed according to Gaussian-Lorentzian functions after subtracting the baseline.

3 Experimental Results

3.1 *Labeling the Raman Spectrum of Human Skin*

Similar to the case of other soft tissues, the Raman spectrum of skin is dominated by the vibrational bands of its structural proteins, amino acids and lipids. Figure 1 shows a Raman spectrum detected by our microprobe equipment with focusing on the stratum corneum of a sample (top-view spectrum) from a 3-month-old donor. Raman spectra from the healthy skin of infants are seldom found in the published literature. For this reason, we have considered this spectrum as a "reference" one since it was almost unaffected by environmental effects. In this study, it is used for a preliminary screening of the emitted Raman bands and to label them according to the published literature.

The Raman spectrum in Fig. 1 has arbitrarily been divided into a low-frequency zone (250 to 1800 cm^{-1}) and a high-frequency zone (2800 to 3200 cm^{-1}). In these two spectral zones, a total of 20 bands could be distinctly observed, as labeled in Fig. 1 (bands 1 to 20). Table 2 summarizes the observed Raman bands and their physical origin in the two noticed spectral zones reported in literature.[17–61] Bands associated with vibrations of amide bonds in polypeptide chains were observed, with the amide I emission being dominated by C═O stretching vibrations and the amide III band by C─N stretching and N─H bending vibrations. The former emission (band 13) at ~1652 cm^{-1} (here often observed, in agreement with other authors, at a slightly

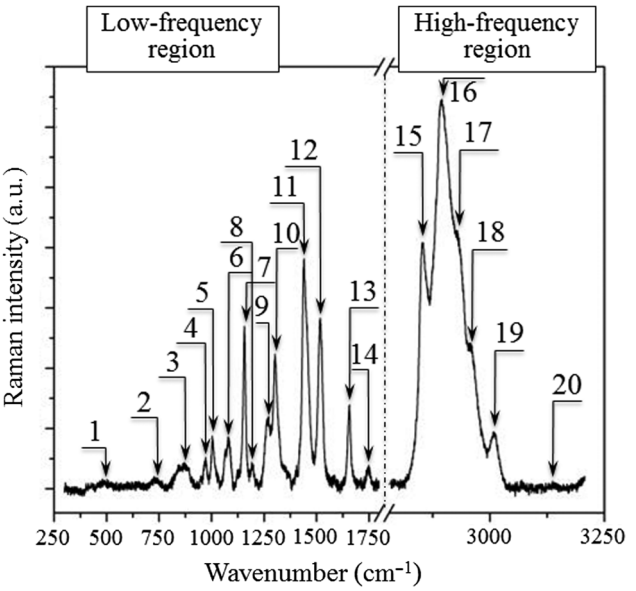

Fig. 1 Raman spectrum as detected with focusing on the stratum corneum of a sample (top-view spectrum) belonging to a 3-month-old infant donor. The spectrum has been arbitrarily divided into low frequency and high frequency zones of investigation. The labeled bands are assigned in Table 2.

higher frequency of 1657 cm^{-1})[23,31,62] is typical of mammalian keratins with mainly α-helical conformation.[18,19,63] On the other hand, the latter emission presented two maxima: one at 1271 cm^{-1} (band 10, assigned to nonpolar fragments with high proline content forming collagen triple helix) and the other at 1244 cm^{-1} (overlapped to band 8 already assigned to tryptophan and phenylalanine) from polar fragments of collagen characterized by a low proline content.[24,31,32] Band 9, which appears as a low-frequency shoulder to the 1271 cm^{-1} band 10, is most likely an overlap of vibrational modes from the adenine and cytosine belonging to the β-sheet structure of amide III (reported at ~1258 cm^{-1})[33] and lipids (reported at ~1255 cm^{-1}).[34] The strong emission detected at ~1440 cm^{-1} (band 11) and the weaker but clearly detectable band at ~1750 cm^{-1} (band 14) can both be assigned to vibrational modes in lipids (with a contribution from proteins, especially in the former band).[17–19,26,32,64] In particular, the former band arises from CH_2 scissoring and CH_3 bending,[35] whereas the latter one mainly represents the C═O stretching mode in lipids and phospholipid molecules.[36,37]

In the high-frequency zone, a broad overlapping emission, contributed by at least five relatively strong bands (bands 15 to 19), could be detected, in addition to a rather weak and isolated band centered at higher frequencies (band 20). In this broad emission, the sub-band labeled as band 15 was centered at around 2855 cm^{-1} and represented the symmetric stretching of lipids in the liquid state.[38] However, band 15 is likely to be overlapped by the C─H symmetric stretching band of collagen centered at ~2850 cm^{-1}.[39] The strongest sub-band in this spectral zone was centered at ~2885 cm^{-1} (band 16). This band has been assigned to symmetric stretching in lipids.[38,40] However, band 16 seemed to show a low-frequency shoulder at around 2881 cm^{-1}, also of protein origin, which we did not explicitly label here. This sub-band shoulder was related to C─H symmetric stretching in collagen.[41] Overlapping effects between lipids and collagen will be discussed in more detail in the following

Table 2 Assignment of Raman bands in skin and skin collagen samples: ν, stretching mode; ν_s, symmetric stretch; ν_{as}, asymmetric stretch; δ, bending mode; and w, wagging mode.

Band label	Band position (cm^{-1})	Principal assignment	References
Band 1	510	ν(S–S) in cysteine	17–19
Band 2	745	Symmetric breathing of tryptophan	21,22
Band 3	877	ν(C–C) in hydroxyproline, δ(tryptophan ring)	18,20,2324–25
Band 4	919	ν(C–C) of proline rings	17,18,26,27
Band 5	1003	ν(C–C) in phenylalanine	17,18,26,27
Band 6	1081	$\nu(CO_3^{2-})$ and $\nu(PO_4^{3-})$, ν(C–C) in lipids	22,24
Band 7	1157	Sphingomyelin	28
Band 8	1208	$\nu(C–C_6H_5)$ in tryptophan and phenylalanine	29,30
Band A^-	1210	$\nu(C–C_6H_5)$ in tyrosine and phenylalanine	35
Band A	1218	Amide III, ν(C–N) and δ(N–H) in α-helix	36,45–49
Band 1*	1242	Amide III, ν(C–N) and $w(CH_2)$ in collagen	65
Band 9	1255, 1258	Amide III, adenine and cytosine β-sheet structure + lipids	33,34
Band 10	1271	Nonpolar fragments of proline in α-helix	24,31,32
Band 3*	1315	Amide III, $\delta(CH_2)$ in α-helix collagen	65
Band B	1338	Amide III, ν(C–N) and δ(N–H) in hydrated α-helix	37
Band C	1370	Ring and ν(C–N) in cytosine and guanine	44
Band D	1395	Symmetric $\delta(CH_3)$ of the methyl groups of proteins	50
Band 11^A	1428	Proteins + lipids, CH_2 scissoring	56–58
Band 11^B	1450	δ(CH) in proteins + lipids	56–58
Band 11^C	1467	$\delta(CH_2)$ in proteins + lipids	56–58
Band 12	1526	Sphingomyelin	28
Band E	1520	ν(C=N) in adenine and cytosine in α-helix	51,52
Band F	1551	Amide II, ν(C–N) and δ(N–H)	53,54
Band G	1584	δ(C=C) in phenylalanine	44
Band H	1605	ν(C=C) in phenylalanine and tyrosine	41,55
Band I	1638	Amide I, ν(C=O) in α-helix + β-sheet	39,56
Band 13	1652	Amide I, ν(C=O) in α-helix	23,31,62
Band J	1681	Amide I, ν(C=O) in disordered structure	40,56
Band 14	1750	ν(C=O) in lipids and phospholipids	36,37
Band 15	2855	$\nu_s(CH_3)$ in lipids (liquid state)	38
Band 16^-	2877	$\nu_s(CH_3)$ in lipids (hexagonal)	60,61
Band 16	2881	$\nu_s(CH_3)$ in lipids (orthorhombic)	56
Band L	2910	$\nu(CH_2)$ and $\nu(CH_3)$ in cholesterol and phospholipids	59

Table 2 (*Continued*).

Band label	Band position (cm^{-1})	Principal assignment	References
Band 17	2928	$\nu_s(CH_3)$ in proteins	42
Band 17$^+$	2950	$\nu_{as}(CH_3)$ in proteins	42
Band 18	2956	$\nu_{as}(CH_3)$ in proteins	42
Band 18$^+$	2980	$\nu(CH^{\alpha,\alpha'})$	41
Band 19	3010	ν_{as}(=C–H) in lipids and unsaturated acids	40,43

sections. Bands 17 and 18 are seen as two consecutive shoulder sub-bands to the overall emission toward higher frequencies. The origin of both these bands, which are located at 2928 and 2956 cm^{-1}, respectively, is probably also a composite one with components from both lipids and collagen. However, the former band corresponds to CH_3 symmetric stretching (i.e., due primarily to proteins),[66] whereas the latter one hits a frequency related to their CH_3 asymmetric stretching.[42] Band 19 is weaker than the other bands composing the overall high-frequency Raman emission, but clearly appears as a more separate sub-band. Its location is at ~3010 cm^{-1}, which corresponds to asymmetric stretching of =C–H groups in lipids, fatty and unsaturated acids.[40,43] Finally, a quite weak but resolvable band was observed at ~3140 cm^{-1}. We labeled it as band 20, and it was tentatively assigned to N–H symmetric stretching.[44]

It has been reported that in tissue, the spectral range from 3200 to 3600 cm^{-1} is occupied by a broad band peaking at ~3250 cm^{-1}, which is associated with O–H stretching vibrations of tissue-bound water and N–H stretching vibrations of proteins.[17,18,32] Conversely, the presence of unbound water (i.e., tetrahedral water clusters) in skin is represented by a band located at 180 cm^{-1} in the Raman spectrum.[67] The status of hydration of skin has been estimated through the intensity ratio between the protein stretching band at 2938 cm^{-1} (which we observed at ~2928 cm^{-1}) and the water stretching band at 3250 cm^{-1}.[67] Raman spectra from skin samples before and after sunlight exposure revealed a total fraction of water higher by ~30% in the latter sample as compared to the former one.[17] We also observed water-related features in our skin samples. However, although it has been recognized that the water content in skin generally increases with age,[68] we ruled out *a priori* the possibility of using the hydration ratio as a meaningful parameter for age assessments because of the strong environmental effects on the hydration state of skin and the fact that each skin layer might show a different hydration level.[69,70] We failed in observing a reliable trend in hydration levels independent of environmental effects and depending on age, probably also because the Raman probe reached different structures while in-depth penetrating samples from donors with different ages, thus giving different intensity ratios. On the other hand, an important hint in this work was that skin-aging processes involve conformational changes in structural proteins. In the Raman spectra of skin samples from older individuals and/or of skin exposed to sunlight, the maxima of the amide I and III bands were systematically detected at spectral positions shifted toward lower frequencies as compared to the spectrum of young and/or unexposed skin samples. Moreover, reduced intensities were generally found and a shift occurred of the CH_2 stretching band in the aliphatic side chains of amino acids toward lower frequencies. This latter spectral perturbation was interpreted as the consequence of structural changes in protein folding.[70,71]

3.2 *Average Raman Spectra as a Function of Donors' Age*

Prior to Raman spectroscopic characterizations, H&E stain histology and optical microscopy were applied on the cross sections of all samples in order to preliminarily assess the location of different zones of epidermis and dermis from morphological features. Figure 2 shows a micrograph of the investigated histological section with the H&E stain of the sample from the 3-month-old infant donor. Labels show the protocol for the line-scan Raman spectroscopy characterization in various regions of the skin at increasing depths. Similar line scans were performed on all the investigated samples from donors of different age.

In this section, we compare typical Raman spectra collected as a function of patient age from the stratum corneum (i.e., at depth from the sample surface, $z = 0$ μm), from a deeper zone in the epidermis zone (just below the stratum corneum, $z = 100$ μm; simply referred to as "epidermis," henceforth) and from a zone further in depth, which was thought to preponderantly be part of the dermis in all the investigated samples ($z = 700$ μm). It should be noted at the outset that the thickness of various zones along the depth of skin significantly varies with location in the body and with age. We have minimized the former difference by sampling always from the same part of the

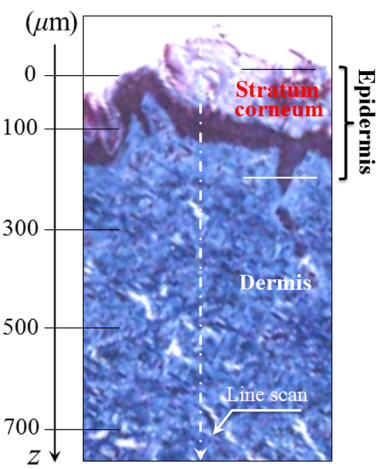

Fig. 2 Skin cross-sectional sample belonging to the 3-month-old donor with H&E stain. Labels illustrate the procedure of Raman microprobe line scan along the in-depth abscissa, z, with origin at the free surface of the sample.

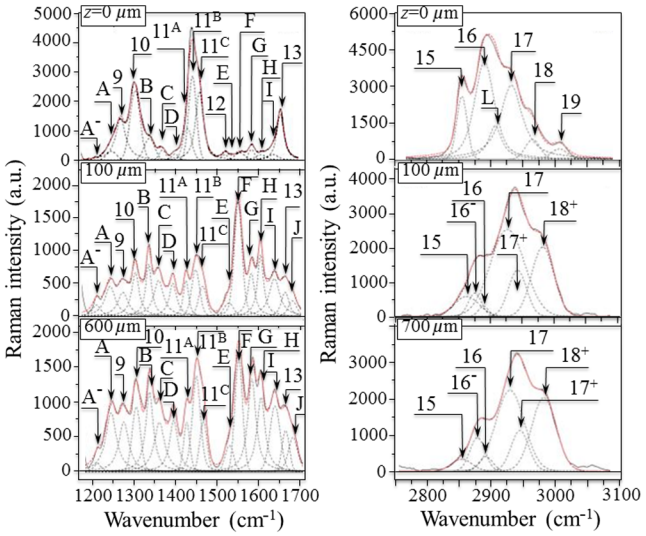

Fig. 3 Average Raman spectrum collected on the skin cross-section sample belonging to a 3-month-old infant. Spectra from both low frequency and high frequency zones are shown as collected at different depths. The origin of the labeled bands is assigned in Table 2.

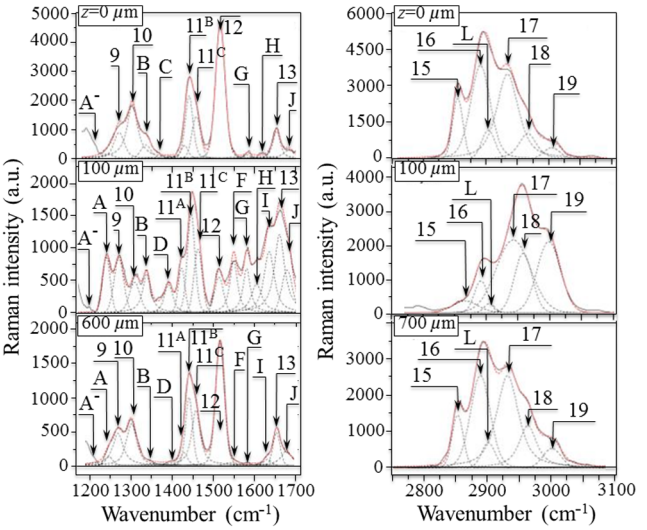

Fig. 5 Average Raman spectrum collected on the skin cross-section sample belonging to a 17-year-old donor. Spectra from both low frequency and high frequency zones are shown as collected at different depths. The origin of the labeled bands is assigned in Table 2.

donors' body (abdomen). However, the latter difference is itself a part of our assessments and yet stems from our sampling. Figures 3–7 show average spectra collected on skin cross-section samples of a 3-month-old infant, 15-, 17-, 35-, and 62-year-old donors, respectively. The recorded spectra showed a significant degree of complexity and there were a large number of features coming out from a comparison of average Raman spectra collected at different locations and from donors with different ages. Table 2 lists all the Raman bands discussed in the remainder of this paper, together with their physical origin.

In the following 10 points, we attempt to rationalize the main features that came to light from the recorded Raman spectra. The main findings can be summarized as follows:

(1) The spectrum acquired in the stratum corneum of the 3-month-old infant was quite different when recorded from the sample surface and from cross section (cf. Figs. 1 and 3). On the low-frequency foot of the 1150 to 1750 cm^{-1} spectral interval, a new band appeared at around 1210 cm^{-1} (labeled band A^- in Fig. 3), which was rather weak in the stratum corneum but became well resolved in both epidermis and dermis spectra. Band A^- was assigned to the stretching mode of $C{-}C_6H_5$ in tyrosine and phenylalanine.[35] Additional new features also appeared in spectra from epidermis and dermis. Although the intensity ratio between band 10 (assigned to nonpolar fragments with high proline content forming collagen triple helix) and band 9 (overlap of vibrational

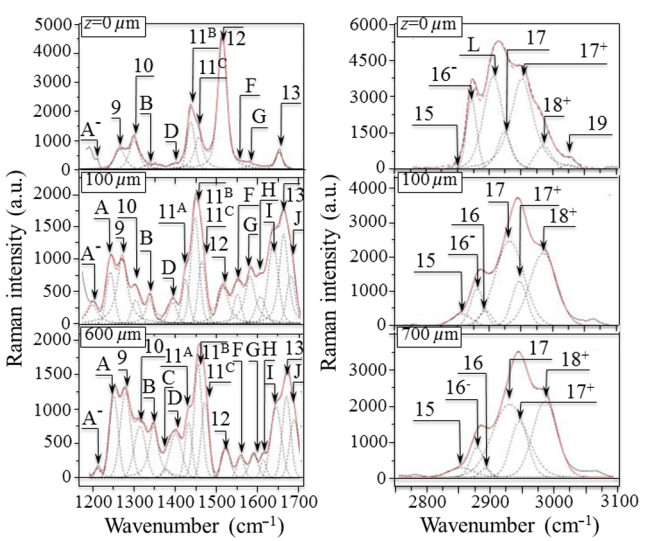

Fig. 4 Average Raman spectrum collected on the skin cross-section sample belonging to a 15-year-old donor. Spectra from both low frequency and high frequency zones are shown as collected at different depths. The origin of the labeled bands is assigned in Table 2.

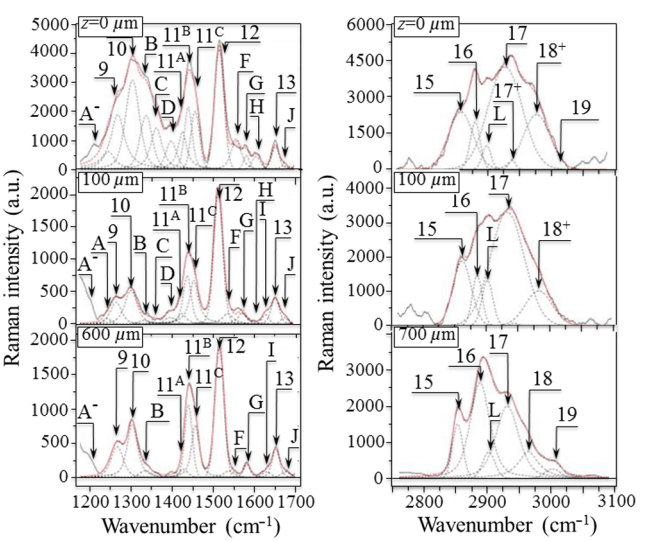

Fig. 6 Average Raman spectrum collected on the skin cross-section sample belonging to a 35-year-old donor. Spectra from both low frequency and high frequency zones are shown as collected at different depths. The origin of the labeled bands is assigned in Table 2.

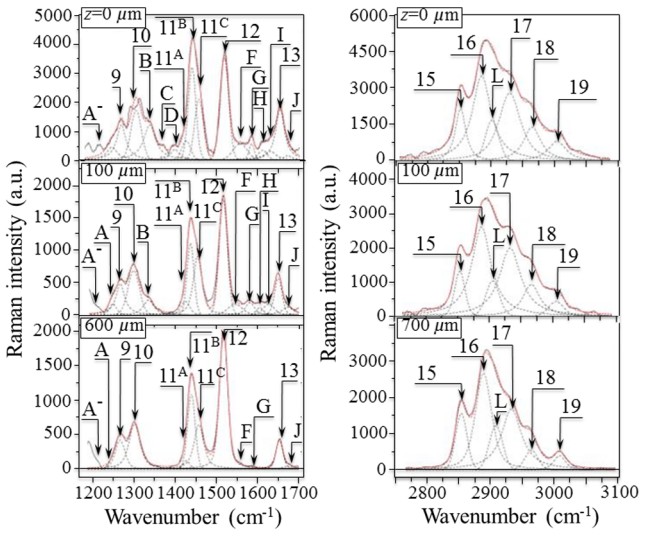

Fig. 7 Average Raman spectrum collected on the skin cross-section sample belonging to a 62-year-old donor. Spectra from both low frequency and high frequency zones are shown as collected at different depths. The origin of the labeled bands is assigned in Table 2.

modes from the adenine and cytosine belonging to the β-sheet structure of amide III and lipids) was similar in the stratum corneum for spectral acquisitions from top surface and cross section, four additional bands appeared in the latter measurements at 1218, 1338, 1370, and 1395 cm^{-1} (labeled as bands A, B, C, and D, respectively, in Fig. 3). Band A was especially pronounced in both epidermis and dermis, quite different from the morphology of a low-frequency shoulder to band 9, as detected in the case of stratum corneum. It was assigned to amide III and, specifically, to coupling of C—N stretching and N—H bending (mixed with vibration of side chains in proteins).[45] Note also that band 9 could be considered as being composed of two distinct sub-bands at lower and higher wavenumbers (at 1243 and 1274 cm^{-1}, respectively). However, these two bands were both assigned to C—N stretching in the α-helix conformation of amide III,[36,46–49] and we neglected their distinction in this study. Band B has also been reported to arise from amide III hydrated α-helix (N—H bending and C—N stretching)[37] and to be partly contributed by tryptophan (CH_2/CH_3 wagging, twisting and bending).[22] Band C was interpreted as ring and C—N stretching in cytosine and guanine,[44] whereas band D arose from symmetric CH_3 bending of the methyl groups of proteins.[50] Bands B, C, and D became extremely pronounced (comparable or even more intense than bands 9 and 10) in both epidermis and dermis spectra of the infant sample (cf. Fig. 3).

(2) The intensity of the sphingomyelin band (band 12) appeared relatively weak in the cross-section spectra of the stratum corneum of the 3-month-old-donor sample (i.e., comparable with that detected on the top surface; cf. Figs. 1 and 3 at $z = 0$). This band did not appear at all in both epidermis and dermis spectra. Another striking feature in the cross-sectional spectra of both epidermis and dermis of the infant sample was a quite pronounced Raman activity in the zone 1550 to 1682 cm^{-1}. While in the spectrum of stratum corneum recorded from the top surface, we could only observe one main band (band 13; related to mammalian keratins with mainly α-helical conformation) in cross section and six additional bands could be observed in this spectral zone (i.e., besides band 13) in both epidermis and dermis. Those bands were centered at ~1520, 1551, 1584, 1605, 1638, and 1681 cm^{-1} (labeled as bands E, F, G, H, I, and J, respectively). Assignments were made, as follows: (1) band E, probably an overlap of (—C=C—) stretching in carotenoid and C=N stretching in adenine and cytosine in α-helix;[51,52] (2) band F, amide II of proteins (N—H bending and C—N stretching);[53,54] (3) band G, C=C bending mode of phenylalanine;[35] (4) band H, protein C=C stretching in phenylalanine and tyrosine;[41,55] (5) band I, amide I band related to both α-helix and β-sheet (C=O stretching vibrations);[39,56] and (6) band J, amide I band related to a disordered structure, nonhydrogen bonds, and C=O stretching.[40,56] Note that band E, which is absent in normal tissues, might be contributed here by carotenoids contained in the infant's artificial milk. Bands F, G, H, and I were also observed in the stratum corneum of the cross-section sample, but with significantly lower intensity. Moreover, band F in the stratum corneum was shifted by few wavenumbers toward higher frequencies as compared to epidermis and dermis spectra.

(3) When collected from cross section, band 11 in the sample from the 3-month-old donor became clearly resolvable into three distinct sub-bands located at 1428, 1450, and 1467 cm^{-1} (labeled 11^A, 11^B, and 11^C, respectively). We have mentioned in the previous section that band 11 can be assigned to vibrational modes in both lipids and proteins. Deconvolution into three distinct sub-bands enabled us to resolve CH_2 scissoring (11^A), C—H bending (11^B), and CH_2 bending (11^C) components.[56–58] In the high-frequency zone of the cross-section spectra from the 3-month-old-infant sample, a comparison with topside spectra showed that the basic structure of five sub-bands was still preserved, but several differences were also spotted. In the stratum corneum, one significant variation was observed in the presence of a new band centered at ~2910 cm^{-1}. This new band, labeled as band L in Fig. 3, was assigned by other authors to CH_3 stretching vibrations in proteins.[66,72] However, there is also a clear overlap with CH_2 and CH_3 stretching contributions from cholesterol, phospholipids and creatine.[59] Significant variations in the relative intensity of various sub-bands could also be recorded. While spectra from the stratum corneum of the infant sample were found, except for the presence of the newly detected band L, to experience a quite similar balance between sub-band intensities when recorded from top surface and cross-section, a significant drop-down was found in both epidermis and dermis spectra for bands 15 and 16 (cf. Fig. 3), which could be assigned to symmetric stretching of liquid-state and crystalline lipids, respectively. This band was relatively strong only in the stratum corneum, whereas a new sub-band

appeared and was labeled as band 16^{-}, at ~2877 cm^{-1} in both epidermis and dermis. We justified the intensity annihilation of band 16 with the low content of lipids in infant skin. The presence of band 16^{-} could then be interpreted according to not only a contribution from collagen (C—H symmetric stretching), but also with the presence of lipids in different physical states. The packing of lipids within skin lamellae is usually referred to as the lateral lipid organization. In the order of increasing packing density, such lipid organization could either be liquid, hexagonal, or orthorhombic.[60] In a healthy human stratum corneum from adult skin, the lipids mainly assemble themselves in an orthorhombic lipid organization at skin temperature, although domains with a hexagonal or liquid organization also exist along the in-depth abscissa.[60,61] In infant skin, the lipid structure is expected to be strongly oriented toward a liquid and a hexagonal package. In substance, the conspicuous intensity reduction in intensity of band 15 in spectra collected upon cross-section sampling enabled resolving the actual structure of what we have detected in topside spectra (cf. Fig. 1) as a cumulative band 16 (seen at around 2881 cm^{-1}). Band 15, the sub-band 16^{-}, band 16, and band L can all be assigned to symmetric stretching of CH_3 units.[56] However, it is hard to distinguish where such CH_3 units exactly belong in the structure of skin. Bands 15 and 16 should mainly arise from CH_3 units embedded in lipids with different physical states, namely liquid and crystalline (i.e., orthorhombic), respectively. Band 16^{-} stems from CH_3 units embedded in collagen, but should also be contributed by lipids in hexagonal packing (i.e., intermediate between liquid and orthorhombic structures). Band L is also a mixed contribution from proteins, cholesterol, phospholipids, and creatine. Additional discussion regarding the fractional contributions of proteins and lipids in this spectral zone will be given in the forthcoming discussion section.

(4) On the high-frequency side of the spectral zone at 2800 to 3200 cm^{-1}, for both epidermis and dermis spectra, the sub-band related to asymmetric stretching of =C—H groups in lipids, fatty and unsaturated acids (band 19) completely disappeared, while a strong band newly appeared at ~2980 cm^{-1} shifted by about 12 cm^{-1} toward higher frequencies as compared to band 18 (cf. Fig. 3). This new sub-band was labeled as 18^{+} and was assigned to $CH_{\alpha,\alpha'}$ stretching.[41] Moreover, band 17 at 2928 cm^{-1}, which corresponds to CH_3 symmetric stretching primarily in proteins, became accompanied by a new sub-band located at ~2950 cm^{-1}, which was labeled as band 17^{+}. This latter band could also be assigned to CH_3 asymmetric stretching in proteins.[42]

(5) As a general trend in the low-frequency region between 1150 and 1750 cm^{-1}, the sample from the infant donor was the one that showed the most marked differences between spectra collected at the three investigated locations, namely at the stratum corneum, epidermis and dermis (i.e., $z = 0$, 100, and 700 μm in depth from the sample surface, respectively). The remaining samples showed less significant variations in the spectral characteristics recorded at different depths with increasing donor's age, with the least variations apparently recorded for the oldest 62-year-old donor (compare Figs. 3 and 7). In particular, the high-frequency part of the spectra in the sample from this latter donor was almost exactly the same at $z = 0$, 100 and 700 μm in depth (cf. Fig. 7) and also exhibited a morphology profile similar to the spectrum recorded from the topside acquisition in the stratum corneum (not shown here). Regarding the low-frequency side of the spectrum from the oldest donor in Fig. 7, the morphology of bands 11 (lipids) and 12 (sphingomyelin) was very similar for detections at different locations in cross section, although their intensity ratios were different. The intensity ratio of band 12 over band 11 (considered as the sum of sub-bands 11^{A}, 11^{B}, and 11^{C}) increased significantly in both epidermis and dermis of the sample from the oldest donor, reaching values ~1.3 to a value ~0.87 in the stratum corneum. Note that in the spectra retrieved from the sample belonging to the youngest donor (cf. Fig. 3), the average ratio between band 12 and band 11 in the stratum corneum was very low, namely ~0.06. Similarly, band 12 was also hardly resolvable in spectra collected from both epidermis (i.e., at $z = 200$ μm) and dermis (at $z = 700$ μm). Another main feature in the spectrum retrieved from the oldest donor investigated was that band B, only pronounced in the stratum corneum, apparently tended to disappear with increasing depth until becoming completely annihilated in the dermis. Band B corresponds to molecular vibrations in amide III hydrated α-helix, in particular N=H bending and C—N stretching. Its full annihilation might thus suggest a drastic reduction of hydrated α-helix in the amide III structure of dermis. Limited to the stratum corneum, the skin of the oldest patient showed a detectable intensity for band G at ~1585 cm^{-1}, while this band also tended to become very weak in the epidermis and almost disappeared in the dermis (cf. Fig. 7). Note that we noticed the inverse trend in the skin sample from the infant donor, namely a conspicuous increase in the intensity of band G in both epidermis and dermis as compared to the stratum corneum. Band G is related to the C=C bending mode of phenylalanine and its decrease suggests a lack of this essential α-amino acid in the skin structure. Phenylalanine is found naturally in the breast milk of mammals, which explains its abundance in the skin sample from the infant donor. Finally, another feature appearing from the comparison between samples from the youngest and the oldest donors was the different intensity of band J in epidermis and dermis (cf. Figs. 3 and 7). This band showed a quite weaker intensity in the older donor as compared to the younger one, a characteristic that confirmed the notion of a more disordered structures for amide I in the skin of infants.

(6) A morphological comparison between epidermis and dermis spectra from skin samples of the 35-year-old and 62-year-old donors showed very few differences, except for a stronger Raman activity in the spectral zone between 1200 and 1400 cm^{-1} in the stratum

corneum of the sample from the former donor (cf. Figs. 6 and 7). Independent of location and unlike the case of the infant donor (cf. Fig. 3), band J was quite weak in samples from both the 35- and 62-year-old donors (cf. Figs. 1 and 7). A pronounced intensity for band J in the epidermis and dermis was also found in samples from both 15- and 17-year-old patients (cf. Figs. 4 and 5). An attempt to rationalize the findings related to band J will be given in the forthcoming discussion section. In the high-frequency zone, the different behavior of band 19 was also resolvable and was more markedly present in the oldest donor. However, samples from both the 15- and 17-year-old donors showed quite different patterns regarding band 19, which seems to be quite affected by the donor habits and lifestyle. Regarding spectra from the stratum corneum and specifically the overlapping set of low frequency bands (A, 9, 10, B, C, and D), a comparison as a function of donors' age revealed tangible morphological differences. However, spectra from the stratum corneum appeared by far the most difficult to rationalize with the same criteria. The spectrum from young donors (3 months, 15 and 17 years old, in Figs. 3–5, respectively) showed low intensities for bands B and C relative to the intensity of band 10. The intensity of these bands increased in the 35-year-old donor (cf. Fig. 6), but it was similar to the infant donor in the spectrum from the 62-year-old donor (Fig. 7). A similar trend was found for the intensity of band D in the stratum corneum. Some inconsistencies between the samples from 15- and 17-year-old donors could be found in the low-frequency spectral zone. Although these donors were close in age, quite different spectral morphologies could be found in the stratum corneum (cf. Figs. 4 and 5). These considerations lead us to the conclusion that low-frequency Raman spectra from the stratum corneum could be less suitable for age analyses due to the strong effect of environmental conditions and individual habits.

(7) The high-frequency part of the Raman spectra in samples from donors of intermediate age was also analyzed in comparison with the two extreme cases of infant and older donors. In dermis spectra, band 18^+ was only present with relatively high intensity in samples from the two youngest donors (Figs. 3 and 4), while it disappeared in samples from the three older donors together with the appearance of band 18 (with intensity decreasing with increasing age) and band 19 (with intensity almost constant with age; cf. Figs. 5–7). Both band 18 (CH_3 asymmetric stretching) and band 18^+ ($CH_{\alpha,\alpha'}$ stretching) are related to vibrational modes in proteins; therefore, the preferential presence of one over the other might serve to specify protein quality in the donor. However, the present data do not seem to allow qualifying whether or not such a feature specifically relates to the donors' ages. For example, in the 35-year-old sample, band 18^+ from $CH_{\alpha,\alpha'}$ stretching was present in the stratum corneum and epidermis, but it disappeared in dermis (cf. Fig. 6). On the other hand, in the infant donor sample, band 18^+ was detected in epidermis and dermis, but it disappeared in the stratum corneum (cf. Fig. 3). In the sample from the 15-year-old donor, band 18^+ appeared at any location (cf. Fig. 4), while it disappeared at any location in samples from the 17- and 62-year-old donors in favor of a clearly resolvable band 18, present at any location along the cross section (cf. Figs. 5 and 7). A meaningful trend with increasing donor age seemed to arise in the variations of Raman intensity in the low-frequency shoulder of the cumulative spectrum at 2800 to 3200 cm^{-1}, namely for the group of bands 15, 16^-, 16, and L. Upon considering the relative intensity of bands (16^-, 16, L) versus band 15, namely the fraction of bands contributed by crystalline lipids versus the one contributed by lipids in the liquid state, a consistent trend showing a tangible increase of the former state with increasing donor age could be observed. A plot and a more detailed discussion of this trend will be given in Sec. 4.2.

(8) Band B, which arises from N—H bending and C—N stretching in amide III hydrated α-helix, seemed to provide a coherently decreasing trend with age in the dermis zone of all the available samples. A decrease in content of hydrated α-helix with increasing age represents a reasonable argument from the viewpoint of ceramide containing structures and skin barrier functions.[73] This trend was less clear (i.e., more scattered) in epidermis spectra and completely absent in a comparison among spectra from the stratum corneum among the investigated samples. This means that environmental factors can also strongly affect hydration of α-helix in portions of skin exposed to sunlight or externally treated. Moreover, dietary effects have also recently been reported in this context, which might alter both dryness and dehydration of the skin.[73] Renugopalakrishnan et al.[74] noticed the amide I emission (i.e., dominated by C═O stretching vibrations and typical of α-helical conformation in mammalian keratin) for spectroscopically evaluating thermal denaturation in chick skin. The used band corresponds to band 13 in Figs. 3–7, which we observed as centered at a frequency of ∼1657 cm^{-1}. Moreover, Tosato et al.[75] discussed band 13 as a sensor for structural modifications of the amide group. The rationale of the discussion was based on the observation that the C═O stretching mode in amide I is weakly coupled to the stretching mode of the carbon–nitrogen bond and to the in-plane deformation mode of the nitrogen–hydrogen amide bond. Accordingly, changes in the molecular geometry due to degradation of collagen triple helix chains might result in the dissociation of the triple helix into a simple string or a double string.[76,77] Band 13 in spectra at any location of our samples showed significant shifts in frequency, but no morphological variations nor any obvious correlation with band B in different samples. On the other hand, again in Ref. 74, the most striking difference of thermal denaturation was observed for the amide III doublet, which we labeled as band 9 (vibrational modes from the adenine and

cytosine belonging to the β-sheet structure of amide III) and band A (coupling of C─N stretching and N─H bonding in amide III). This doublet collapsed upon denaturation to produce a strong band at lower frequencies at around 1243 cm^{-1}. We also noticed a collapse of band A in dermis spectra with increasing age, but no similar trend could be observed for band 9. Moreover, no strong new band could be detected at around 1243 cm^{-1}. Following Renugopalakrishnan et al.,[74] the collapse of band A could, in principle, be interpreted as a signal of incipiency for a denaturation process of protein and polypeptides in the amide III structure, which progressively occurs with increasing age.

(9) The lipidic content of skin is a key factor in the permeability barrier function, including cosmetics effects and transdermal drug delivery. Abnormalities in barrier function, which are related to lipid content, have been shown to lead to atopic dermatitis and other common cutaneous diseases.[78] Free fatty acids and triglycerides are affected in their compositions by ultraviolet irradiation,[79] and a decrease in lipid content with age leads to an increased susceptibility to exogenous insults.[80] These latter two aspects are essential to our research because they show that if the effect of environmental factors could be separated, a detailed spectroscopic knowledge of lipidic content, composition, and structure might not only help to elucidate skin function, malfunction and abnormality, but it could also be a marker of the actual age of skin. An early study by Ghadially et al.[80] showed that fatty acids in senescent murine epidermal lipids are clearly different from young controls, since they contain a disproportionate increase in medium and long chain species. On the other hand, no changes were apparent in very long chain species. Moreover, in both aged human and mouse epidermis, a paucity of secreted lamellar body contents was present at the stratum granulosum/stratum corneum interface, a finding that matched the lipid biochemical observation showing that lipids in aged stratum corneum are globally reduced in quantity, without exhibiting any specific abnormality in species distribution or fatty acid composition. A former study by Gaber and Peticolas[38] suggested the use of the Raman activity of lipids in the spectral interval between 2850 and 2890 cm^{-1} (our bands 15 and 16) for assessing the physical state of phospholipids. As we have discussed in point (4), we detected in this study a clear monotonic variation with donors' ages of the Raman activity in this high-frequency region, which suggests the presence of lipids in an increasingly crystalline state (over liquid and semicrystalline states) in donors with increasing age. On the other hand, if we look at the lipid/protein activity in the low-frequency region, as represented by bands 11^A, 11^B, and 11^C at around 1440 cm^{-1}, we could not find any monotonic trend with increasing age at any investigated location. This trend is probably due to the fact that both lipids and proteins contribute to the three sub-bands. This point will be discussed in more detail in the initial subsection of the forthcoming discussion. Moreover, the balance between the intensity of various sub-bands was barely altered as a function of age and location (cf. Figs. 3–7). Translating the above set of information into physical arguments, our experiments prove that band 11, which "feels" local motifs encoded into the primary structure of lipids and proteins [i.e., CH_2 scissoring (11^A), C─H bending (11^B), and CH_2 bending (11^C)], is not strongly affected by age; but, regarding lipids, it is their physical state that monotonically changes with progressing age, namely bands 15 and 16, which reflect the tertiary structure of the lipid molecules, actually undergo a progressive crystallization process of lipid assembly in older patients.

(10) The Raman activity in the interval of frequencies from 1600 to 1700 cm^{-1} typically appeared as a triplet (bands I, 13, and J), with bands 13 and I being the most prominent in the stratum corneum and in epidermis or dermis, respectively. As already mentioned, band 13 has unambiguously been assigned to the amide I vibrational mode,[81] which mainly involves C═O stretching and, to a lesser extent, N─H in-plane bending of peptide groups.[82,83] The exact spectral location of this band strongly depends on the secondary structure of the polypeptide chain and could, therefore, be useful for estimating secondary structure fractions of proteins.[84] In comparing epidermis and dermis spectra from the oldest and the youngest donors in this study, band 13 was found to be clearly shifted towards lower frequencies in the former donor. Regarding samples from donors with intermediate age, the sample from the 35-year-old donor displayed band 13 at nearly the same frequency as the sample from the 62–year-old donor. On the other hand, band 13 from both samples from the 15- and 17–year-old donors was very close in frequency to that of the infant donor. Despite a possible interaction with vibrational modes in lipids, a strong intensity of band 13 in the Raman spectra should testify to a preponderance of proteins with high α-helix content.[82,83,85] On the other hand, band I, which comprises amide I contributions from both α-helix and β-sheet (C═O stretching vibrations) is more difficult to interpret.[39,56] A spectral shift toward lower frequencies of bands 13 and I could be interpreted as a mark for the presence of heavier structures in α-helix and β-sheet, and thus for a larger interaction with lipids. The spectral intensity of band J, which encompasses all the amide I contributions from disordered structures, nonhydrogen bonds, and C═O stretching,[40,56] to the sum of α-helix-representative band 13 and α-helix and β-sheet-related band I can be assumed as a direct measure of the degree of disorder of the protein structure in the tissue. Our data showed that in epidermis and dermis, the intensity of band J with respect to band 13 seemed to decrease with increasing age, although its absolute value apparently depended on individual donors. This point will be discussed in more detail in the forthcoming sections. In principle, there could also be another additional spectral feature that characterizes the fractional

presence of β-sheet structures. This is a band appearing at around 1517 cm^{-1}, which mainly involves N—H in-plane bending and C—N stretching of the trans peptide group of amide II vibrations.[81] However, this band was hardly observed in this study. According to a study by Shao et al.,[86] dealing with structural changes in heated up proteins upon interaction with lipids, the increase of β-sheet formation is due to proteins–lipids and proteins–proteins interactions during environmental exposure. In general, the behavior of Raman bands related to peptides and proteins, also including the band at 1517 cm^{-1}, in the stratum corneum is not necessarily intrinsic to the skin structure but might be altered by environmental conditions. For this reason, we have neglected it in our further characterizations.

According to the spectral characterizations shown above, we monitored the following spectral features:

(1) the intensity ratio of band 10 on band 9, I_{10}/I_9, representative of the fractional ratio between α-helix and β-sheet;

(2) the intensity ratio of band J on band 13, I_J/I_{13}, representative of the fractional ratio between disordered and ordered structures (in peptides and proteins);

(3) the intensity ratio of band 12 on band 11^B, I_{12}/I_{11^B}, representative of the content of sphingomyelin as compared to the overall amount of lipids in the sample;

(4) the intensity ratio of band 16 on band 15, I_{16}/I_{15}, representative of the physical state of lipids, namely liquid versus crystalline state; and

(5) the spectral shift of band 13, ω_{13}, representative of changes in molecular geometry of amide I, due to the degradation of collagen triple helix chains and their dissociation into simple or double strings.

More information about the variation of these five factors along the in-depth axis on cross sections of the investigated skin samples is available in the Appendix, and the dependence of these parameters on age will be further discussed in the following section.

4 Discussion

4.1 *Subtracting from Skin Spectra the Contribution of Standard Collagen*

The Raman spectrum of dermis is dominated by collagen, which in turn constitutes 70% of the dry weight and 90% of the total protein content. Important contributions to the Raman spectrum of skin are also expected in the stratum corneum and in the epidermis zones. Of the about 20 types of collagen existing in the human body, skin consists of ~80% type I and 15% type III, while the remaining 5% is predominantly type IV collagen.[87–89] Figure 8 shows the Raman spectrum of skin (type I) collagen purchased from Sigma-Aldrich Co, which was collected under exactly the same experimental conditions as the spectra of skin as shown in Figs. 3–7.

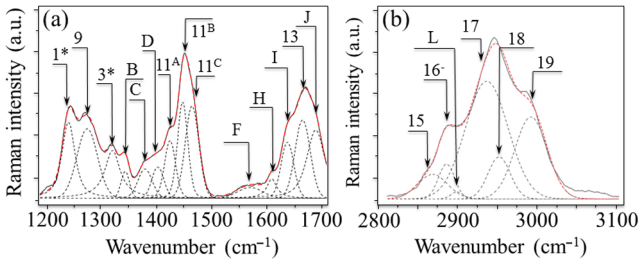

Fig. 8 Raman spectrum of skin (type I) collagen in (a) low and (b) high frequency regions, which was collected under exactly the same experimental conditions as that the spectra of skin. The labeled bands are assigned in Table 2.

On the low-frequency side of the spectrum, as shown in Fig. 8(a), most of the bands could be labeled, similar to what was detectable in the skin samples (cf. Table 2). The relatively strong intensity of the C—H vibration bands (11^A, 11^B, and 11^C) in skin collagen suggests that the contribution of collagen to their overall intensity in skin samples is not negligible as compared to the respective contributions in lipids. Only two additional bands (i.e., bands 1* and 3*) remained to be assigned; these bands were not obviously detectable in the skin samples as they appeared on the low-frequency side of the collagen spectrum. Band 1* was centered at around 1242 cm^{-1} and could be related to amide III disordered structures (C—N stretching and CH_2 wagging), whereas band 3*, at 1315 cm^{-1}, was again related to α-helix amide III (CH_2 bending mode).[65]

Regarding the high-frequency side of the Raman spectrum of pure collagen, we have collected six distinct bands (labeled as 15, 16^-, 17–19 and L) with an overall morphology comparable to that found in skin spectra. However, non-negligible shifts (toward lower or higher wavenumbers) could be found for some bands. Interestingly, band L was quite weak, thus suggesting a preponderant contribution of lipids over proteins. Moreover, band 16, observable in skin, could not be found in the collagen spectrum. The important implication in these findings is that band 15 and band 16^- as observed in the skin sample, which were assigned to symmetric stretching of CH_3 units in lipids embedded in phases with different physical states, also exist in collagen with the same physical origin, but appearing at shifted frequencies. In an attempt to better visualize this complex spectroscopic situation, we normalized the high-frequency side of the skin spectra to the respective intensity maxima along the cross-section scan (in Figs. 3–7), and from them we subtracted the contribution of the similarly normalized collagen spectrum (Fig. 8). The results of this procedure are shown in Fig. 9 for spectra belonging to the youngest and to the oldest donors in this study [spectra from the 3-month- and 62-year-old donors in (a) and (b), respectively]. In the plots, the Raman intensity difference, $\Delta I = I_s - I_c$, is plotted as a function of spectral locations, where I_s and I_c represent the normalized intensities of skin and collagen spectra, respectively. In each figure, three plots are given which correspond to different depths along the z-axis, namely $z = 0$ (stratum corneum), $z = 100$ μm (epidermis), and $z = 700$ μm (dermis). In the plots, positive and negative values for ΔI correspond to a preponderance of lipids or collagen contributions to the skin spectra, respectively. For better clarity, the spectral location of these bands, belonging to collagen, is also shown in insets of both figures.

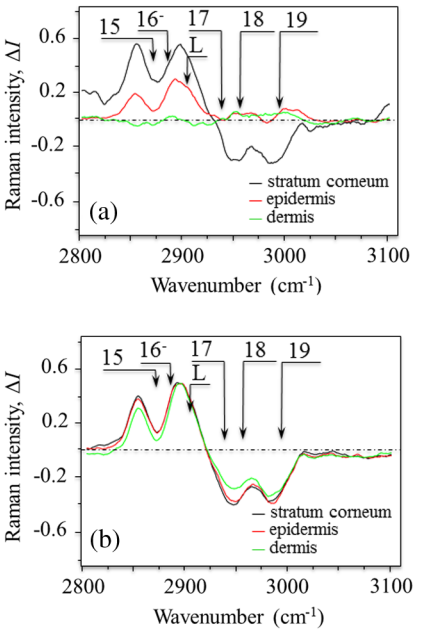

Fig. 9 Raman intensity difference, $\Delta I = I_s - I_c$, as a function of spectral locations, as calculated after spectral normalization to the respective intensity maxima; the plots refer to the 3-month- and 62-year-old donors [in (a) and (b), respectively]. Three plots are displayed for each donor, which represent averages over the stratum corneum, epidermis and dermis.

The following conclusions could be drawn as the main outputs of the spectral subtraction procedure:

(1) The Raman spectrum from the dermis zone of the skin sample was completely composed of type I collagen in the case of the infant donor [cf. $\Delta I \sim 0$ over the entire high frequency zone in Fig. 9(a)]. However, increasingly pronounced spectral contributions from lipids could be noticed at 2800 to 2930 cm^{-1} when proceeding along the cross-section line-scan toward the surface of the sample.

(2) In the Raman spectrum from the 62-year-old donor, from surface to $z = 700$ μm, subtraction of the collagen spectrum from the skin spectrum produced the same results, independent of location along the line scan. Lipids were preponderant in the spectral interval 2800 to 2930 cm^{-1}, while the main spectral contribution at higher frequencies mainly stemmed from type I collagen structures [cf. Fig. 9(b)].

(3) The spectral subtraction procedure, showing that the band labeled as 16^- in skin corresponded to C—H symmetric stretching in collagen, has provided an important confirmation about the possibility of using bands 15 and 16 (centered at ~2855 and ~2885 cm^{-1}, respectively) for discussing the physical state of lipids in skin. However, discussions on lipid structures using the above two bands should be limited to the stratum corneum and epidermis, since their contributions in the spectrum from dermis were, in young donors, completely contributed by collagen structures.

4.2 *Possible Spectroscopic Parameters for Evaluating Human Age*

Our attempts "to decode" skin spectra in search for a possible natural "clock" in the vibrational behavior of skin have brought us several hints concerning the evolution of the chemical and physical nature of proteins and lipids with age. Figure 10 shows plots of different selected parameters as a function of donors' ages.

As previously discussed, the intensity ratios I_{10}/I_9 and I_J/I_{13} can be considered as representative of the fractional ratio between the α-helix and β-sheet, and of the fractional ratio between disordered and ordered structures (in peptides and proteins), respectively. The plots in Figs. 10(a) and 10(b) display these (average) parameters as a function of donors' ages. In the averaging process, we have excluded the stratum corneum in order to minimize environmental effects. The trend for I_{10}/I_9 in the former plot, when averaged on different areas of the cross section of the samples, showed a minimum for the 17-year-old donor. This clearly nonmonotonic nature was more pronounced in the epidermis than in the stratum corneum. We have similarly found nonmonotonic plots (not shown here) for other parameters [e.g., the sphingomyelin ratio, I_{12}/I_{11^B}], as proposed above. On the other hand, the plot of I_J/I_{13} versus donors' ages remarkably fitted to a high degree of precision with an exponential decrease in donors' ages. According to our data, the algorithm relating the Raman intensity ratio I_J/I_{13} to age, x_A, can be given as

$$I_J/I_{13} = 0.74 \times \mathrm{Exp}[-0.048 \times x_A]. \quad (1)$$

The notion of folding and misfolding in peptides and proteins is a well-known one in the field of biophysics.[90–92] In order to become functionally active, newly made (or "nascent") protein chains must assemble into a "fold," namely a well defined 3-D pattern. An amino acid sequence specifies the information that specifies the fold, which is a process thermodynamically driven

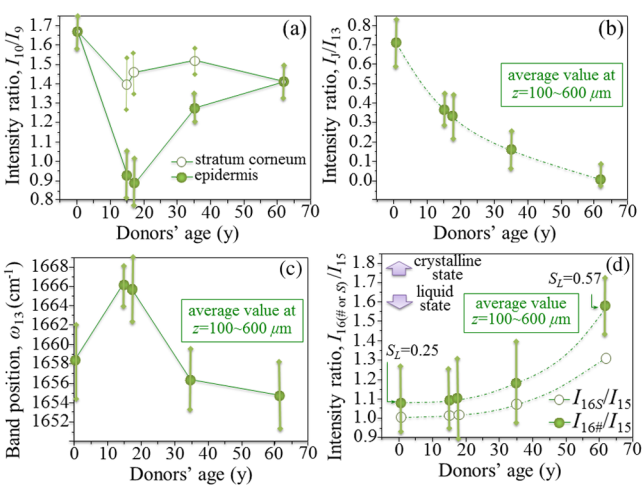

Fig. 10 Plots of different parameters as a function of donors' ages: the intensity ratio, I_{10}/I_9, (a) representative of the fractional ratio between α-helix and β-sheet; the ratio, I_J/I_{13}, (b) representative of protein folding upon aging; the spectral shift of band 13, ω_{13}, (c) representative of the amount of rupture of triple helix molecules within the collagen macromolecule due to degradation of collagen type IV; and (d) the ratios of $I_{16\#} = I_{16^-} + I_{16} + I_L$ to I_{15} and $I_S = I_{16^-} + I_{16}$ to I_{15} as representative of the process of lipid crystallization upon aging.

by the hydrophobic effect. Structural rearrangement gives rise to the correct amino acid packing that corresponds to the most stable and active state in healthy subjects. This task is completed within intervals of time between milliseconds and many minutes, depending on protein size. On the other hand, band 13, in the region at around 1659 cm^{-1}, is associated with the triple-stranded helix stabilized in collagen by a large number of interchain hydrogen bonds.[93] Fourier transform infrared spectroscopy data by Federman et al.[94] have assessed band displacements from the 1652 toward 1658 cm^{-1}, which indicates the rupture of the triple helix molecule within the collagen macromolecule due to degradation of collagen type IV by the metalloproteinase trypsin. In other words, the plot in Fig. 10(c), which shows the spectral displacements of band 13 as a function of age, is another aspect of protein changes related to aging. It should be noted that in the case of collagen, newly synthesized premature collagen is imported into the lumen of endoplasmic reticulum and folded and modified during transportation through the Golgi apparatus and is then secreted as a mature form. During this protein maturation, misfolded proteins are subjected to degradation. Mature proteins are also degraded when damaged. This protein metabolism can be affected by both age and environmental stress. The protein state in the skin should thus be the result of both synthesis and degradation, which is altered in an age-dependent manner, so young skin contains a higher amount of fresh collagen than old.

In conclusion, our data in Fig. 10(b) simply show that the amount of proteins in skin, which are yet to assembly into folds, is largest in infants and gradually reduces with aging. This circumstance is thus the spectroscopic representation of the fact that the dermis of newborns contains less mature collagen than adults. Moreover, Fig. 10(c) shows that stabilization of the triple helix is maximized at intermediate ages, a behavior that is in good agreement with the maximization of α-helix contents testified by the concurrent minimum of the intensity ratio, I_{10}/I_9[Fig. 10(a)]. In other words, as far as proteins are concerned, Raman spectroscopic data have provided us with a consistent picture of structural evolution with age which is in agreement with well-established concepts in biophysics of the aging process.

Regarding lipids, we show here another spectroscopic plot which apparently contained characteristics of remarkable precision with respect to the evolution with increasing age. This plot is shown in Fig. 10(d) and represents the relationship found between the first two maxima appearing in the high-frequency zone investigated at around 2885 and 2890 cm^{-1}. In epidermis and dermis, the presence of more crystallized and ordered structures (i.e., a decreasing trend for the I_J/I_{13} ratio) through aging corresponds to a general and well-established notion in biophysics.[95–97] We plotted, in Fig. 10(d), both the ratio of $I_{16\#} = I_{16^-} + I_{16} + I_L$ to I_{15} and the ratio of $I_S = I_{16^-} + I_{16}$ to I_{15}. Both plots show a similar trend of exponential increase with increasing age, although the former plot gives a more distinct separation between young and old donors. Note also that the former plot could be preferable to the latter one because it just represents the ratio between the first two maxima in correspondence of the lower foot of the high-frequency zone of the skin spectrum; thus, it does not require any spectral deconvolution procedure to be calculated. Interestingly, a plot that simply uses the intensity of the deconvoluted band 16 to band 15 leads to the opposite trend (i.e., a decreasing ratio with age; cf. Figs. 11 and 12 in Appendix). This finding, together with the observation of the remarkably low intensity of band L in collagen, suggests the preponderance of the lipid contribution (i.e., cholesterol, phospholipids and creatine) of band L in skin samples. Following the definition given by Gaber and Peticolas,[38] we defined the order parameter for lateral interaction, S_L, according to the following equation:

$$S_L = \frac{(I_{16\#}/I_{15}) - 0.7}{1.5}, \tag{2}$$

which refers to lipids in fully crystalline and fully liquid states when equal to 1 and 0, respectively. This parameter, given in the inset of Fig. 10(d), reflects the intermolecular structure of lipids and decreases in the order from lamellar liquid, hexagonal liquid crystal and orthorhombic crystal state. According to our data, an empirical equation that represents the Raman intensity ratio, $I_{16\#}/I_{15}$, as a function of age, x_A, can be drawn, as follows:

$$I_{16\#}/I_{15} = 1.06 \times \mathrm{Exp}[0.00028 \times x_A^{1.75}] \tag{3}$$

or, alternatively, in terms of the order parameter, S_L:

$$S_L = 0.707 \times \mathrm{Exp}[0.00028 \times x_A^{1.75}] - 0.467. \tag{4}$$

4.3 *Needs for the Raman Probe in Forensic Assessments of Human Age*

A reliable estimation of age at death, which is a main element in the identification of bodies of unidentified origin, is also one of the main challenges in forensic sciences. For example, official data from Kyoto Prefecture[98] report an average number of ~13 persistently unidentified human bodies per year in the last 12 years. Such a large number of cases for a limited geographical area could give an idea of the severity of this problem from the social side. A number of anthropological techniques have been put forward to estimate the age at death in children and adults, but they are obviously insufficient in a number of cases. These techniques include long-bone length, epiphyseal fusion, dental eruption, and lengths of diaphysis at birth for infant and juvenile remains; eruption of third molars, fusion of the spheno-occipital synchondrosis, pubic symphysis, auricular surface, cranial sutures, sternal rib ends (costal cartilage), maxillary suture closure, tooth-root translucency, and formation of osteoarthritis characteristics in adults (for a complete review of these methods, see Ref. 99). However, two main shortcomings appear in applying these methodologies: (1) an increasingly lower accuracy for adult subjects and (2) the absolute necessity of specific references depending on population. In order to overcome these deficiencies, new methodologies have been developed, which have so far included both biochemical and chemical methods. The former methods basically consist of screening the natural processes of aging, thus including different biochemical changes that lead to alterations in cells and tissues. Biochemical methods have so far relied on forensic analyses of hair, drugs in hair blood, and semen, based on infrared spectroscopy, chromatography, ultraviolet, and mass spectrophotometry.[100] The chemical methods, on the other hand, involve manipulation and modifications of molecules or accumulation of selected products as, for example, modifications that take place in DNA and chromosomes. Among the chemical methods, the most accurate

technique today is considered to be aspartic acid racemization in noncollagenous bone proteins or tooth enamel,[101,102] although other techniques are being concurrently used depending on the forensic context under examination.[103] In this paper, we have described a Raman approach to age evaluation on skin samples which basically belongs to the biochemical type of analyses since it requires no sample manipulation except for the extraction of a skin sample from the ventral part of the body. Although Raman spectroscopy could, in principle, also be applied *in situ* without any physical extraction of a skin sample from the body, our study has clearly shown how crucial it is to obtain cross-sectional skin samples in order to retrieve more detailed spectral information on protein and lipid structures and to avoid biases of environmental nature unavoidably contained in the stratum corneum (i.e., on the top surface) of the skin sample. Although less established as compared to radiographic analyses,[104,105] Raman spectroscopy has been widely used in different branches of forensic science.[106,107] However, studies using the Raman method for age assessments are few and are based on phenomenological approaches.[108,109] In Ref. 109, the authors used a correlation between the variability of Raman spectra and the stages of dentinal evolution with advancing age and remarkably obtained predictions of a correct age, with a mean error of ± 5 years. The main benefit of this method consisted of minimal and nondestructive sample preparation, which in turn led to an efficient age prediction for any age group. From this viewpoint, our study of skin presents a similar advantage but also necessitates more detailed and physics-driven Raman analyses of organic molecules. The very least outputs of our study are a complete labeling of Raman bands in cadaveric samples of skin (including an infant), their spectral deconvolution and their different trends with age as a function of in-depth abscissa. Despite the limited number of cadaveric samples investigated, which unavoidably limits the nature of this investigation to a proof-of-concept study, the Raman response of proteins and lipids in skin samples seemed to remarkably obey precise patterns, consistent with general biophysical concepts. Thus, Raman spectroscopy seems to provide a reliable and more straightforward path to age determination as compared to other spectroscopic techniques involving electrons, microscopic forces or neutrons.[110–113]

5 Conclusion

The aim of this work was to establish a correlation between age and Raman spectra retrieved from human skin. We explored both top-surface and cross-sectional Raman responses in skin samples from cadaveric donors of different ages and found the latter spectra more meaningful and richer in structural details than the former ones, regarding both proteins and lipids. Clear correlations could be found between the relative intensity of selected Raman bands and the stages of protein folding and evolution of lipid crystallization with advancing age. Protein folding seems to be a more sensitive parameter for infants and young patients, while lipid crystallization follows more sensitive variations with age for patients in their adulthood. It is probable that an algorithm combining both these two spectral parameters could improve the precision of age estimation. Moreover, there were hints for the presence of additional "biological clocks" in the Raman spectrum of skin. However, the complexity of the retrieved spectra poses considerable challenges to additional findings. Although a limited number of only five cadaveric donors that were available for our experiments necessarily confines our data into a mere proof-of-concept frame, the degrees of protein folding and lipid crystallization seemed to represent precise predictors of biological age. While we hope that our findings will stimulate other researchers to prove the newly stated concepts, additional experiments are going on in our laboratory to enlarge the number of donors every time they become available to us. The proposed Raman method should especially be suitable for those kinds of situations where traditional methods fail and a prompt and minimally invasive evaluation of age is needed.

Appendix

Profiles along the in-depth axis on cross sections of the skin samples. Figures 11 and 12 show line-scan plots of these spectroscopic parameters as a function of distance, z, from the surface of the skin sample. Plots are displayed for samples from the 3-month- and 62 year-old donors in Fig. 11, whereas Fig. 12 compares the results obtained from samples belonging to the 15-year- and 35-year-old donors. For brevity's sake, data from the 17-year-old donor were not explicitly shown, since they were very similar to those collected on the sample from the 15-year-old sample. As discussed in the manuscript, the intensity ratios I_{10}/I_9 and I_J/I_{13} [displayed in Figs. 11(a) and 11(e), and 12(a) and 12(e)] were considered as representative of the fractional ratio between α-helix and β-sheet and of the fractional ratio between disordered and ordered structures (in peptides and proteins), respectively. A comparison between the youngest and the oldest donors in this study [i.e., as displayed in Figs. 11(a) and 11(e)] revealed a similar in-depth distribution for the ratio I_{10}/I_9, while the trends for the ratio I_J/I_{13} were quite different. Leaving aside data from the stratum corneum (strongly affected by environmental effects), we examined data collected in the epidermis and dermis region. In these zones, the I_J/I_{13} ratio was almost constant at ~0.7 for the infant sample, while it was ~0 in the sample from the old donor. This finding was interpreted with the presence of a more crystallized and ordered structure in the older donor as compared with the infant donor. Looking at the samples from the donors of intermediate age [in Figs. 12(a) and 12(e)], the trend of a decreasing I_J/I_{13} ratio (i.e., of an increased crystallinity and structural order) in both epidermis and dermis with increasing age seemed to be confirmed. Moreover, the ratio I_{10}/I_9 also experienced lower values at intermediate ages as compared to both samples from the youngest and oldest donors. The ratio I_{12}/I_{11^B} was monitored [cf. Figs. 11(b), 11(f), 12(b), and 12(f)] because it was thought to represent the content of sphingomyelin as compared to the overall amount of lipids in the sample. The amount of sphingomyelin showed a trend that was not monotonic with donors' ages. It was highest in the deep portions of the sample from the 35-year-old donor, while the minimum value was detected in the infant sample.

Sphingomyelin (also referred to as ceramide phosphorylcholine) consists of a ceramide unit with an attachment of phosphorylcholine moiety. Although sphingolipids are the main polar lipid constituents of milk, they represent an important but minor nutrient for infants, which justifies the low level found for this sphingolipid in the sample from the infant donor. Holleran et al.[114] have shown that sphingolipids, including sphingomyelin, represent ~25% of the lipids located in the stratum corneum and are a major element of the epidermal

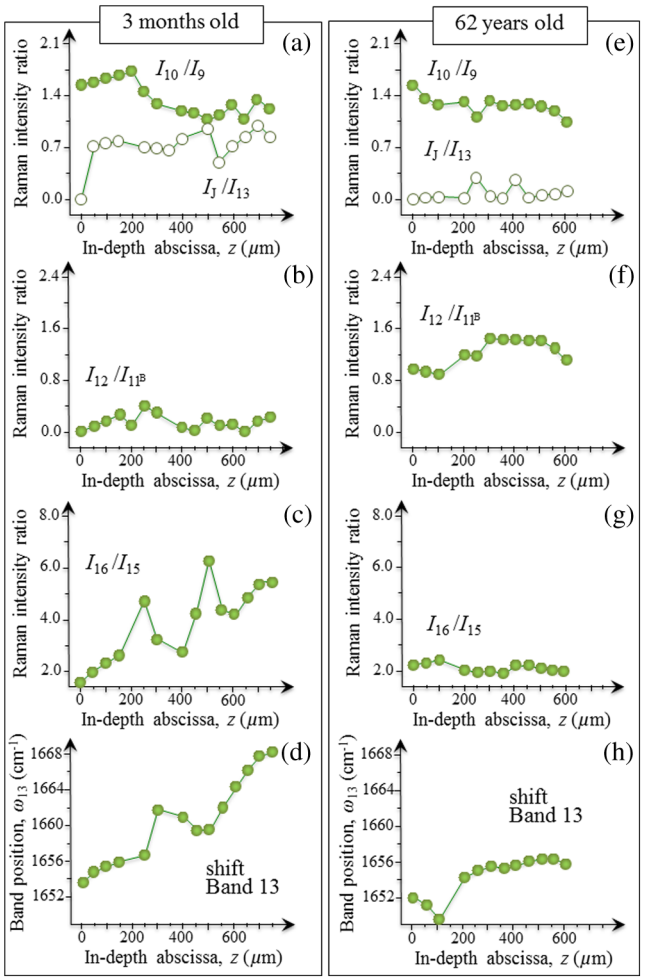

Fig. 11 Line-scan plots as a function of distance, z, from the surface of the skin sample comparing the trends found for the 3-month [(a) to (d)] and the 62-year-old donor [(e) to (h)]. Plots show the intensity ratio of band 10 on band 9, I_{10}/I_9 and the intensity ratio of band J on band 13, I_J/I_{13} [in (a) and (e)]; the intensity ratio of band 12 on band 11^B, I_{12}/I_{11^B}[in (b) and (f)]; the intensity ratio of band 16 on band 15, I_{16}/I_{15} [in (c) and (g)]; and, the spectral shift of band 13, ω_{13} [in (d) and (h)].

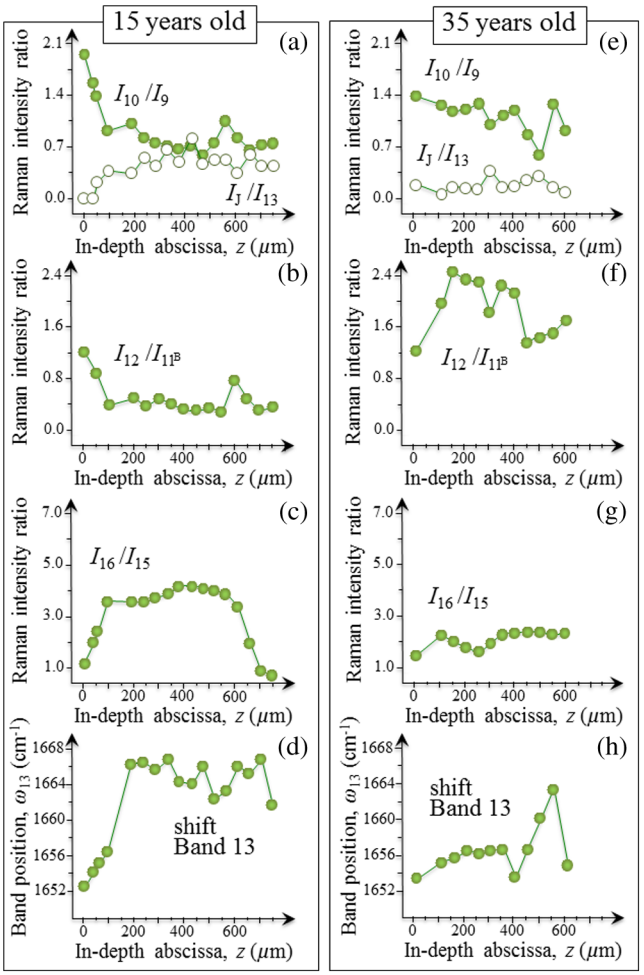

Fig. 12 Line-scan plots as a function of distance, z, from the surface of the skin sample comparing the trends found for the 15-year-old [(a) to (d)] and the 35-year-old donor [(e) to (h)]. Plots show the intensity ratio of band 10 on band 9, I_{10}/I_9 and the intensity ratio of band J on band 13, I_J/I_{13} [in (a) and (e)]; the intensity ratio of band 12 on band 11^B, I_{12}/I_{11^B}[in (b) and (f)]; the intensity ratio of band 16 on band 15, I_{16}/I_{15} [in (c) and (g)]; and, the spectral shift of band 13, ω_{13} [in (d) and (h)].

permeability barrier. Moreover, alterations in epidermal barrier function lead to a rapid increase in cholesterol and fatty acid synthesis, which parallels the early stages of the repair process. Sphingolipid synthesis was also found to increase during barrier repair but with a delayed response in comparison to cholesterol and fatty acid synthesis.[115] Since a deficiency of any of these species will result in abnormal membrane structures with a reduced capacity to impede trans-epidermal water flux,[116] our findings here might simply show that such a protective capacity in skin is maximized in the medium age of humans, initially increasing from infant age and then again turning back to low levels for advanced ages.

Figures 11(c), 11(g), 12(c), and 12(g) show the line-scan trends retrieved for the Raman intensity ratio I_{16}/I_{15}, which is representative of the physical state of lipids, namely liquid versus crystalline state. A comparison between the youngest and oldest donors [Figs. 11(c) and (g)] shows a clearly positive gradient up to high values of this intensity ratio (i.e., up to 5 to 6) as a function of in-depth abscissa, z, in the former sample, versus a conspicuously constant (and low) value ~2 in the latter sample. Samples from donors from intermediate ages [Figs. 12(c), and 12(g)] also showed intermediate trends with conspicuously constant values in large portions of both the epidermis and dermis. High I_{16}/I_{15} ratios represent a preponderance of crystalline lipids over liquid ones, which conceivably accompany the increase in age in humans. Interestingly, a similar trend could be obtained from retrieving the spectral shifts, ω_{13}, for band 13 as a function of the abscissa, z [cf. Figs. 11(d), 11(h), 12(d), and 12(h)]. A gradual increase as a function of the abscissa, z, was found for the infant donor versus a lesser increase up to lower frequencies in the oldest donor. Intermediate trends appeared in samples from donors of intermediate ages. As discussed in the paper, the shift of band 13 toward higher frequencies has been considered to represent changes in the molecular geometry of amide I due to degradation of collagen triple helix chains and their dissociation into simple or double strings. Higher frequencies, such as those being observed in younger donors, thus might represent a higher fraction of unfolded structures in young skin samples, as also suggested by the higher values of the I_J/I_{13} ratio. On the other hand, shifts toward low wavenumbers have been interpreted as the effect of the squeezing out of water (and a

consequent reinforcement of hydrogen bonds) between adjacent chains in a study of keratin fibers under strain by Paquin and Colomban.[65] This interpretation leads us to consider a higher chain packing in adult skin samples, which is also a reasonable output when considering the chemistry of skin aging.

References

1. W. J. Netzer and F. U. Hartl, "Recombination of protein domains facilitated by co-translational folding in eukaryotes," *Nature* **388**, 343–349 (1997).
2. A. Barth and C. Zscherp, "What vibrations tell about proteins?" *Q. Rev. Biophys.* **35**, 369–430 (2002).
3. J. J. L. Lippert and W. L. Peticolas, "Laser Raman investigation of the effect of cholesterol on conformational changes in dipalmitoyl lecithin multilayers," *Biochim. Biophys. Acta* **282**, 8–17 (1972).
4. Y. M. Weng et al., "Structural analysis of triacylglycerols and edible oils by near-infrared Fourier transform Raman spectroscopy," *Appl. Spectrosc.* **57**, 413–418 (2003).
5. M. F. Mrozek and M. J. Weaver, "Detection and identification of aqueous saccharides by using surface-enhanced Raman spectroscopy," *Anal. Chem.* **74**, 4069–4075 (2002).
6. R. J. Weesie et al., "Semiempirical and Raman spectroscopic studies of carotenoids," *Biospectroscopy* **5**, 19–33 (1999).
7. K. Maquelin et al., "Identification of medically relevant microorganisms by vibrational spectroscopy," *J. Microbiol. Methods* **51**, 255–271 (2002).
8. K. De Gussem et al., "Raman spectroscopic study of Lactarius spores (Russulales, Fungi)," *Spectrochim. Acta A* **61**, 2896–2908 (2005).
9. H. G. M. Edwards et al., "Non-destructive analysis of pigments and other organic compounds in lichens using Fourier-transform Raman spectroscopy: a study of Antarctic epilithic lichens," *Spectrochim. Acta A* **59**, 2301–2309 (2003).
10. V. Baeten, "Raman spectroscopy in lipid analysis," *Lipid Technol.* **22**(2) 36–38 (2010).
11. J. De Gelder et al., "Reference database of Raman spectra of biological molecules," *J. Raman Spectrosc.* **38**, 1133–1147 (2007).
12. G. J Thomas, Jr., "Raman spectroscopy of protein and nucleic acid assemblies," *Annu. Rev. Biophys. Biomol. Struct.* **28**, 1–27 (1999).
13. C. Raschke and P. Elsner, "Skin aging: a brief summary of characteristic changes," in *Textbook of Aging Skin*, M. A. Farage, K. W. Miller, and H. I. Maibach, Eds., pp. 37–44, Springer-Verlag, Berlin (2010).
14. F. H. Silver, *Mechanosensing and Mechanochemical Transduction in Extracellular Matrix Biological Chemical Engineering and Physiological Aspects*, Springer, New York (2006).
15. J. Rosenbloom, W. R. Abrams, and R. Mecham, "Extracellular matrix 4: the elastic fiber," *FASEB J.* **7**(13), 1208–1218 (1993).
16. Sigma Aldrich, "Life science," http://www.sigmaaldrich.com/life-science/metabolomics/enzyme-explorer/learning-center/structural-proteins/collagen.html.
17. M. Gniadecka et al., "Structure of water proteins and lipids in intact human skin hair and nail," *J. Invest. Dermatol.* **110**, 393–398 (1998).
18. W. Akhtar and H. G. M. Edwards, "Fourier-transform Raman spectroscopy of mammalian and avian keratotic biopolymers," *Spectrochim. Acta A* **53**, 81–90 (1997).
19. H. G. M. Edwards, A. C. Williams, and B.W. Barry, "Potential applications of FT-Raman spectroscopy for dermatological diagnostics," *J. Mol. Struct.* **347**, 358–379 (1995).
20. R. Manoharan, Y. Wang, and M. S. Feld, "Histochemical analysis of biological tissues using Raman spectroscopy," *Spectrochim. Acta* **52**, 215–249 (1996).
21. N. Stone et al., "Near-infrared Raman spectroscopy for the classification of epithelial pre-cancers and cancers," *J. Raman Spectrosc.* **33**, 564–573 (2002).
22. W. T. Cheng et al., "Micro-Raman spectroscopy used to identify and grade human skin pilomatrixoma," *Microsc. Res. Tech.* **68**(2), 75–79 (2005).
23. R. Dong et al., "Temperature-dependent Raman spectra of collagen and DNA," *Spectrochim. Acta A* **60**, 557–561 (2004).
24. W. T. Cheng et al., "Micro-Raman spectroscopy used to identify and grade human skin pilomatrixoma," *Microsc. Res. Tech.* **68**(2), 75–79 (2005).
25. M. Polomska et al., "Fourier transform near infrared Raman spectroscopy in studies on connective tissue," *Acta Phys. Pol. A* **118**(1), 136–140 (2010).
26. M. G. Shim and B. C. Wilson, "Development of an in vivo Raman spectroscopic system for diagnostic applications," *J. Raman Spectrosc.* **28**, 131–142 (1997).
27. H. G. M. Edwards et al., "NIR-FT Raman spectroscopy as a diagnostic probe for mummified skin and nails," *Vibr. Spectrosc.* **28**, 3–15 (2002).
28. S. M. Ali et al., "Raman spectroscopic analysis of human skin tissue sections ex-vivo: evaluation of the effects of tissue processing and dewaxing," *J. Biomed. Opt.* **18**(6), 061202 (2013).
29. Z. Huang et al., "Near-infrared Raman spectroscopy for optical diagnosis of lung cancer," *Int. J. Cancer* **107**, 1047–1052 (2003).
30. Z. Huang et al., "Raman spectroscopy in combination with background near-infrared autofluorescence enhances the in vivo assessment of malignant tissues," *Photochem. Photobiol.* **81**, 1219–1226 (2005).
31. F. S. Parker, *Application of Infrared Raman and Resonance Raman Spectroscopy in Biochemistry*, Plenum Press, New York (1983).
32. T. M. Greve, K. B. Andersen, and O. F. Nielsen, "ATR-FTIR FT- NIR and near-FT-Raman spectroscopic studies of molecular composition in human skin in vivo and pig ear skin in vitro," *Spectroscopy* **22**(6), 437–457 (2008).
33. P. R. T. Jess et al., "Early detection of cervical neoplasia by Raman spectroscopy," *Int. J. Cancer* **121**, 2723–2728 (2007).
34. R. K. Dukor, "Vibrational spectroscopy in the detection of cancer," in *Handbook of Vibrational Spectroscopy* Vol. 5, pp. 3335–3359, John Wiley & Sons, Ltd, Chichester (2002).
35. D. P. Lau et al., "Raman spectroscopy for optical diagnosis in the larynx: preliminary findings," *Lasers Surg. Med.* **37**, 192–200 (2005).
36. N. Stone et al., "Raman spectroscopy for identification of epithelial cancers," *Faraday Discuss.* **126**, 141–157 (2004).
37. R. E. Kast et al., "Raman spectroscopy can differentiate malignant tumors from normal breast tissue and detect early neoplastic changes in a mouse model," *Biopolymer* **89**, 134–141 (2008).
38. B. P. Gaber and W. L. Peticolas, "On the quantitative interpretation of biomembrane structure by Raman spectroscopy," *Biochim. Biophys. Acta* **465**, 260–268 (1977).
39. R. Calheiros et al., "Antioxidant phenolic esters with potential anticancer activity: a Raman spectroscopic study," *J. Raman Spectrosc.* **39**, 95–107 (2008).
40. G. Shetty et al., "Raman spectroscopy: evaluation of biochemical changes in carcinogenesis of oesophagus," *Br. J. Cancer* **94**, 1460–1464 (2006).
41. H. Schultz and M. Baranska, "Identification and qualification of valuable plant substances by IR and Raman spectroscopy," *Vib. Spectrosc.* **43**, 13–25 (2007).
42. R. Agarwal, P. Tandon, and V. D. Gupta, "Phonon dispersion in poly (dimethylsilane)," *J. Organomet. Chem.* **691**, 2902–2908 (2006).
43. C. Krafft et al., "Near-infrared Raman spectroscopy of human brain lipids," *Spectrochim Acta A Mol. Biomol. Spectrosc.* **61**(7), 1529–1535 (2005).
44. G. I. Dovbeshka et al., "FTIR spectroscopy studies of nucleic acid damage," *Talanta* **53**, 233–246 (2000).
45. M. Gniadecka et al., "Diagnosis of basal cell carcinoma by Raman spectroscopy," *J. Raman Spectrosc.* **28**, 125–129 (1997).
46. R. Heckel et al., "Characteristic infrared spectroscopic patterns in the protein bands of human breast cancer tissue," *Vib. Spectrosc.* **27**, 165–173 (2001).
47. S. Sigurdsson et al., "Detection of skin cancer by classification of Raman spectra," *IEEE Trans. Biomed. Eng.* **51**, 1784–1793 (2004).
48. A. Singha et al., "Quantitative analysis of hydrogenated diamond-like carbon films by visible Raman spectroscopy," *J. Appl. Phys.* **100**, 1–8 (2006).
49. A. R. Viehoever et al., "Organotypic raft cultures as an effective in vitro tool for understanding Raman spectral analysis of tissue," *Photochem. Photobiol.* **78**, 517–524 (2003).
50. H. P. Wang, H. C. Wang, and Y. J. Huang, "Microscopic FTIR studies of lung cancer cells in pleural fluid," *Sci. Total Environ.* **204**, 283–287 (1997).
51. Y. G. Hu, A. G. Shen, and T. Jiang, "Classification of normal and malignant human gastric mucosa tissue with confocal Raman

microspectroscopy and wavelet analysis," *Petrochem. Acta A Mol. Biomol. Spectrosc.* **69**, 378–382 (2008).
52. G. I. Dovbeshka et al., "Surface enhanced IR absorption of nucleic acids from tumor cells: FTIR reflectance study," *Biopolymer* **67**, 470–486 (2002).
53. Y. Fukuyama et al., "A study on the differences between oral squamous cell carcinimas and normal oral mucosas measured by Fourier transform infrared spectroscopy," *Biospectroscopy* **5**, 117–126 (1999).
54. Q. B. Li et al., "Diagnosis of gastric inflammation and malignancy in endoscopic biopsies based on Fourier transform infrared spectroscopy," *Clin. Chem.* **51**, 346–350 (2005).
55. J. W. Chan et al., "Micro-Raman spectroscopy detects individual neoplastic and normal hematopoietic cells," *Biophys. J.* **90**, 648–656 (2006).
56. R. J. Lakshimi et al., "Tissue Raman spectroscopy for the study of radiation damage: brain irradiation of mice," *Radiat. Res.* **157**, 175–182 (2002).
57. T. Richter et al., "Identification of tumor tissue by FTIR spectroscopy in combination with position emission tomography," *Vib. Spectrosc.* **28**, 103–110 (2002).
58. E. O. Faolain et al., "A study examining the effects of tissue processing on human tissue sections using vibrational spectroscopy," *Vib. Spectrosc.* **38**, 121–127 (2005).
59. M. Huleihel et al., "Novel optical method for study of viral carcinogenesis in vitro," *J. Biochem. Biophys. Methods* **50**, 111–121 (2002).
60. J. A. Bouwstra et al., "Phase behavior of lipid mixtures based on human ceramides: coexistence of crystalline and liquid phases," *J. Lipid Res.* **42**(11), 1759–1770 (2001).
61. F. Damien and M. Boncheva, "The extent of orthorhombic lipid phases in the stratum corneum determines the barrier efficiency of human skin in vivo," *J. Invest. Dermatol.* **130**, 611–614 (2010).
62. F. M. Lyng et al., "Vibrational spectroscopy for cervical cancer pathology from biochemical analysis to diagnostic tool," *Exp. Mol. Pathol.* **82**, 121–129 (2007).
63. A. N. C. Anigbogu et al., "Fourier transform Raman spectroscopy of interactions between the penetration enhancer dimethyl sulfoxide and human stratum corneum," *Int. J. Pharm.* **125**, 265–282 (1995).
64. L. Knudsen et al., "Natural variations and reproducibility of in vivo near-infrared Fourier transform Raman spectroscopy of normal human skin," *J. Raman Spectrosc.* **33**, 574–579 (2002).
65. R. Paquin and P. Colomban, "Nanomechanics of single keratin fibres: a Raman study of the α-helix $\rightarrow$ β-sheet transition and water effect," *J. Raman Spectrosc.* **38**, 504–514 (2007).
66. N. J. Kline and P. J. Treado, "Raman chemical imaging of breast tissue," *J. Raman Spectrosc.* **28**, 119–124 (1997).
67. M. Gniadecka, O. F. Nielsen, and H. C. Wulf, "Water content and structure in malignant and benign skin tumours," *J. Mol. Struct.* **661–662**, 405–410 (2003).
68. N. Nakagawa and M. Matsumoto, and Sakai, "In vivo measurement of the water content in the dermis by confocal Raman spectroscopy," *Skin Res. Technol.* **16**, 137–141 (2010).
69. S. Fendel and B. Schrader, "Investigation of skin and skin lesions by NIR-FT-Raman spectroscopy," *Fresenius J. Anal. Chem.* **360**, 609–613 (1998).
70. M. Egawa, T. Hirao, and M. Takahashi, "In vivo estimation of stratum corneum thickness from water concentration profiles obtained with Raman spectroscopy," *Acta Dermatol. Venereol.* **87**(1), 4–8 (2007).
71. S. Olsztynska-Janus et al., "Spectroscopic techniques in the study of human tissues and their components. Part II: Raman spectroscopy," *Acta Bioeng. Biomech.* **14**(4), 121–133 (2012).
72. P. J. Caspers et al., "In vivo confocal Raman microspectroscopy of the skin: Non-invasive determination of molecular concentration profiles," *J. Invest. Dermatol.* **116**, 434–442 (2001).
73. T. Oda et al., "Effect of oral intake of ceramide-containing acetic acid bacteria on skin barrier function," *Antiaging Med.* **7**(5), 50–54 (2010).
74. V. Renugopalakrishnan et al., "Non-uniform triple helical structure in chick skin type I collagen on thermal denaturation: Raman spectroscopic study," *Z. Naturforsch.* **C53**(5–6), 383–388 (1998).
75. M. G. Tosato et al., "Raman spectroscopic investigation of the effects of cosmetic formulations on the constituents and properties of human skin," *Photomed. Laser Surg.* **30**, 85–91 (2012).
76. J.-H. Choi and M. Cho, "Calculations of intermode coupling constants and simulations of amide I, II, and III vibrational spectra of dipeptides," *Chem. Phys.* **361**, 168–175 (2009).
77. M. Gniadecka et al., "Water and protein structure in photoaged and chronically aged skin," *J. Invest. Dermatol.* **111**, 1129–1132 (1998).
78. K. R. Feingold, "The importance of lipids in cutaneous function," *J. Lipid Res.* **48**, 2529–2530 (2007).
79. E. J. Kim et al., "UV decreases the synthesis of free fatty acids and triglycerides in the epidermis of human skin in vivo, contributing to development of skin photoaging," *J. Dermatol. Sci.* **57**, 19–26 (2010).
80. R. Ghadially et al., "The aged epidermal permeability barrier: Structural, functional, and lipid biochemical abnormalities in humans and a senescent murine model," *J. Clin. Invest.* **95**, 2281–2290 (1995).
81. S. Krimm and J. Bandekar, "Vibrational spectroscopy and conformation of peptides, polypeptides, and proteins," *Adv. Protein Chem.* **38**, 181–365 (1986).
82. A. M. Herrero, "Raman spectroscopy a promising technique for quality assessment of meat and fish: a review," *Food Chem.* **107**, 1642–1651 (2008).
83. E. C. Y. Li-Chan, "The applications of Raman spectroscopy in food science," *Trends Food Sci.Technol.* **7**, 361–370 (1996).
84. M. Bouraoui, S. Nakai, and E. C. Y. Li-Chan, "In situ investigation of protein structure in Pacific whiting surimi and gels using Raman spectroscopy," *Food Res. Int.* **30**, 65–72 (1997).
85. A. J. P. Alix, G. Pedanou, and M. Berjot, "Determination of the quantitative secondary structure of proteins by using some parameters of the Raman amide I band," *J. Mol. Struct.* **174**, 159–164 (1988).
86. J.-H. Shao et al., "Evaluation of structural changes in raw and heated meat batters prepared with different lipids using Raman spectroscopy," *Food Res. Int.* **44**, 2955–2961 (2011).
87. P. J. Caspers et al., "In vitro and in vivo spectroscopy of human skin," *Biospectroscopy* **4**, S31–S39 (1998).
88. A. Tfayli et al., "Discriminating nevus and melanoma on paraffin-embedded skin biopsies using FTIR microspectroscopy," *Biochim. Biophys. Acta* **1724**, 262–269 (2005).
89. F. H. Silver, J. W. Freeman, and D. DeVore, "Viscoelastic properties of human skin and processed dermis," *Skin Res. Technol.* **7**, 18–23 (2001).
90. V. N. Uversky, C. J. Oldfield, and A. K. Dunker, "Intrinsically disordered proteins in human diseases: introducing the D2 concept," *Annu. Rev. Biophys.* **37**, 215–246 (2008).
91. A. L. Fink, "Protein aggregation: folding aggregates, inclusion bodies and amyloid," *Folding Des.* **3**(1), R9–R23 (1998).
92. P. Leandro and C. M. Gomes, "Protein misfolding in conformational disorders: rescue of folding defects and chemical chaperoning," *Mini Rev. Med. Chem.* **8**, 901–911 (2008).
93. E. Ly et al., "Polarized Raman microspectroscopy can reveal structural changes of peritumoral dermis in basal cell carcinoma," *Appl. Spectrosc.* **62**, 1088–1094 (2008).
94. S. Federman, L. M. Miller, and I. Sagi, "Following matrix metalloproteinases activity near the cell boundary by infrared micro-spectroscopy," *Matrix Biol.* **21**, 567–577 (2002).
95. B. D. McKersie and J. E. Thompson, "Lipid crystallization in senescent membranes from cotyledons," *Plant Physiol.* **59**, 803–807 (1977).
96. D. M. Small, "Progression and regression of atherosclerotic lesions. Insights from lipid physical biochemistry," *Arterioscler. Thromb. Vasc. Biol.* **8**, 103–129 (1988).
97. K. Matsuzaki, "Physicochemical interactions of amyloid β-peptide with lipid bilayers," *Biochem. Biophys. Acta Biomembr.* **1768**(8) 1935–1942 (2007).
98. Kyoto Prefecture, www.pref.kyoto.jp/fukei/sodan/kansiki/fumei/h26/index.htlm.pref.kyoto.jp/fukei/sodan/kansiki/fumei/h26/index.htlm
99. H. M. Garvin et al., "Developments in forensic anthropology: age-at-death estimation," Chapter *10 in A Companion to Forensic Anthropology*, 1st ed., D. C. Dirkmaat, Ed., pp. 202–223, Wiley-Blackwell Publishing Ltd., Chichester, West Sussex, United Kingdom (2012).
100. P. H. Whitehead, "Biochemical techniques in forensic science," *Trends Biochem. Sci.* **10**(8), 299–302 (1985).
101. S. Ritz, A. Turzynski, and H. W. Schutz, "Estimation of age at death based on aspartic acid racemization in noncolagenous bone proteins," *Forensic Sci. Int.* **69**(2), 149–159 (1994).

102. P. M. Helfman and J. L. Bada, "Aspartic acid racemization in tooth enamel from living humans," *Proc. Nat. Acad. Sci. U. S. A.* **72**(8), 2891–2894 (1975).
103. E. Baccino and A. Schmitt, "Determination of adult age at death in the forensic context," Chapter 11 in *Forensic Anthropology and Medicine: Complementary Sciences from Recovery to Cause of Death*, A. Schmitt, E. Cunha, and J. Pinheiro, Eds., pp. 259–280, Humana Press Inc., Totowa, New Jersey, United States (2006).
104. S. I. Kvaal et al., "Age estimation of adults from dental radiographs," *Forensic Sci. Int.* **74**, 175–185 (1995).
105. T. H. Hsiao, H. P. Chang, and K. M. Liu, "Sex determination by discriminant function analysis of lateral radiographic cephalometry," *J. Forensic Sci.* **41**(5), 792–795 (1996).
106. A. H. Kuptsov, "Applications of Fourier transform Raman spectroscopy in forensic science," *J. Forensic Sci.* **39**(2), 305–318 (1994).
107. M. Clayboum and M. Ansell, "Using Raman spectroscopy to solve crime: inks, questioned documents and fraud," *Sci. Justice* **40**(4), 261–271 (2000).
108. A. Osmani, O. Gamulin, and M. Vodanovic, "Age estimation of teeth with Raman spectrometry: preliminary study," *Bull. Int. Assoc. Paleodontol.* **8**(1), 137–143 (2014).
109. P. Tramini et al., "A method of age estimation using Raman microspectrometry imaging of the human dentin," *Forensic Sci. Int.* **118**(1), 1–9 (2001).
110. F. Kosa, A. Antal, and I. Farkas, "Electron probe microanalysis of human teeth for the determination of individual age," *Med. Sci. Law* **30**(2) 109–114 (1990).
111. S. Strasser et al., "Age determination of blood spots in forensic medicine by force spectroscopy," *Forensic Sci. Int.* **170**, 8–14 (2007).
112. K. L. Spalding et al., "Forensics: age written in teeth by nuclear tests," *Nature* **437**, 333–334 (2005).
113. B. A. Buchholz and K. L. Spalding, "Year of birth determination using radiocarbon dating of dental enamel," *Surf. Interfaces Anal.* **42**, 398–401 (2010).
114. W. M. Holleran et al., "Serine-palmitoyl transferase activity in cultured human keratinocytes," *J. Lipid Res.* **31**(9), 1655–1661 (1990).
115. W. M. Holleran et al., "Regulation of epidermal sphingolipid synthesis by permeability barrier function," *J. Lipid Res.* **32**(7), 1151–1158 (1991).
116. W. M. Holleran et al., "Sphingolipids are required for mammalian epidermal barrier function: inhibition of sphingolipid synthesis delays barrier recovery after acute penetration," *J. Clin. Invest.* **88**, 1338–1345 (1991).

Giuseppe Pezzotti is full tenured professor and leader of the Ceramic Physics Laboratory at the Kyoto Institute of Technology, Japan. He graduated summa cum laude in mechanical engineering from Rome University "La Sapienza," Italy, he holds three doctoral degrees in materials engineering, solid state physics, and medical sciences, and is author/coauthor of 570 scientific papers, 1 book, 13 book chapters, and 8 patents, including a world patent on nanoscale stress microscopy in the scanning electron microscope.

Marco Boffelli is a third year PhD student in material science at Kyoto Institute of Technology. He joined professor Pezzotti's research group in 2012 after receiving his diploma in material science from the Ca' Foscari University in Venice in the same year. His research interest includes ceramic biomaterials synthesis and characterization mainly with Raman spectroscopy, scanning electron microscopy, and cathodoluminescence.

Daisuke Miyamori is a lecturer in the Department of Forensic Medicine, Kyoto Prefectural University of Medicine (KPUM). He graduated from Kyushu University. He was working at the emergency department of Shonankamakura Tokushukai Hospital before he got his position at KPUM. He is a licensed medical doctor and specialized in emergency medicine.

Takeshi Uemura is a lecturer in the Department of Forensic Medicine, Kyoto Prefectural University of Medicine (KPUM). He graduated from Toho University and the Graduate School of Pharmaceutical Science, Chiba University. He was working at Arizona University before he got his position at KPUM. He has a pharmacist license. He has been doing his main research about polyamine. Here, he is studying the relationship between polyamine and age.

Yoshinori Marunaka, MD, PhD, is professor and chairperson in the Departments of Molecular Cell Physiology and Bio-Ionomics, Kyoto Prefectural University of Medicine, Japan. He is director and professor at the Japan Institute for Food Education and Health and St. Agnes' University. He is the president-elect of the Physiological Society of Japan, and Editor-in-Chief of the *Journal of Physiological Sciences*. His current research focuses on roles of H+ and Cl- in cell function, including cell growth, neurite elongation, diabetes mellitus etc.

Wenliang Zhu got his PhD in material sciences in Kyoto Institute of Technology in 2005 and is now a lecturer in the Medical School of Osaka University. His main research field is on the development and application of high resolution photo-/electrostimulated spectroscopies for quantitative analysis of structural, mechanical, and chemical properties in single crystalline and polycrystalline ceramics.

Hiroshi Ikegaya is a professor and chairman of the Department of Forensic Medicine, Kyoto Prefectural University of Medicine (KPUM). He graduated from Miyazaki Medical College and Graduate School of Medicine, The University of Tokyo. He was working at National Research Institute of Police Science before he got his position at KPUM. He has a medical doctorate and architect license. He has been doing his main research about development of individual identification methods.